

Dynamics By Design: a Novel Tool for the Kinetic Control of DNA Reaction Systems

BIOREGEN Final Report

Department of Bioengineering
Imperial College London

*A Project Report Submitted in
Partial Fulfilment of the
MEng Biomedical Engineering & Molecular Bioengineering Degrees*

Word Count: 5000

Supervisor:
Dr. Thomas Ouldridge

Department of Bioengineering
t.ouldridge@imperial.ac.uk

April, 2025

BIOREGEN Final Project Report

Simi Brainch, Joseph Mustapha, Nikita James, Sofia Hospodar,
Mikal Semere, Rhianne Henderson, Kaixuan Huang

April 15, 2025

Abstract

DNA, with its predictable base-pairing and ease of design, offers a powerful medium to replicate the behaviours of biomolecular systems. As a result, DNA-based logic has been increasingly used as a means by which to construct complex nanoscale circuits. However, attaining tuneable reaction kinetics in large DNA-based systems remains a key challenge. In this report, we outline a novel method for fine-tuning the rate constants of DNA strand displacement reactions by strategically introducing base-pair mismatches into the binding sites between complexes; overhanging regions known as toeholds. To achieve this, we develop a modular system based on the principles of DNA toehold exchange and use *in silico* tools such as NUPACK to present an analysis of our system. Furthermore, we compile a comprehensive database of our toehold designs, demonstrating that they have the potential to span a complete set of experimentally feasible reaction rates. Additionally, we identify limitations of current modelling methods and discuss their implications for our system. Overall, this work expands the molecular programming toolkit; provides a means by which researchers and engineers can achieve greater kinetic control over their DNA-based systems; and paves the way for the development of dynamic biomolecular systems with applications in diagnostics, synthetic biology, and nanomaterials.

1. Introduction

DNA-based systems naturally exhibit a variety of complex behaviours which allow for the precise regulation of dynamic biological systems. Harnessing this intrinsic programmability has allowed for the construction of systems including nanoscale structures [1, 2, 3]; sensors [4]; molecular motors and DNA-based fuels [5, 6, 7, 8, 9, 10, 11, 12]; and other complex circuitry [13, 14, 15, 16, 17]. DNA is particularly powerful for engineering such nanoscale circuits due to its predictable Watson-Crick base-pairing, structural versatility, well-characterised thermodynamic properties, and ease of sequence design [18, 19, 20, 21, 22]. Combined with its ability to interact with other nanomaterials [23], DNA serves as a prime tool for the design of complex molecular systems.

Due to the high versatility of DNA, diverse architec-

tural setups have been used to program using DNA-based systems. In this report, we focus on strand displacement reactions and their role in dynamic DNA nanotechnologies. In this type of reaction, an invader strand binds to a double-stranded DNA complex and displaces one of the existing strands (the incumbent) through a process called branch migration. This begins at an overhanging single-stranded region called a toehold, which acts as the initiation site for displacement. Once bound, the invader progressively replaces the incumbent, resulting in the formation of a new, more stable, duplex [24]. In the case where the final duplex results in the creation of a new overhanging toehold region, this reaction is known as toehold exchange [25].

1.1. Toehold Exchange Strand Displacement Reactions

Toehold exchange strand displacement [25] is a type of reaction which allows programmable control over molecular interactions by relying solely on predictable base-pairing rules.

In toehold exchange, the invader and incumbent strand both share a complementary domain on the substrate strand. As the invader binds and initiates branch migration, it displaces the incumbent strand ([Figure 1](#)). However, unlike in other types of strand displacement, the completion of the reaction does not result in the permanent loss of one of the two initial toehold regions; instead, a functional toehold is effectively passed from one end of the substrate strand to the other. This mechanism allows the reaction to proceed in both the forward and reverse direction as a function of strand concentrations and thermodynamic conditions. This reversibility, and retention of the toehold domain, provide greater control over reaction kinetics and makes toehold exchange ideal for applications that require repeatable behaviour or downstream secondary reactions that make use of the newly uncovered secondary toehold region, denoted as α in [Figure 1](#) [25].

1.2. Strand Displacement: Implementation of Logical & Dynamic Systems

Strand displacement reactions, including toehold exchange systems, have already been used to successfully construct many complex systems. Recent advances include the construction of elaborate digital logic circuits composed of cascading DNA reactions [26], nanorobot technology [27, 28, 29], and implementations of neural network computation [30, 31, 32, 33]. One recent example of dynamic computation which could be implemented using strand displacement reactions is the Recurrent Neural Chemical Reaction Network (RNCRN) [34], which combines machine learning with chemical dynamics to approximate any system of well-behaved ordinary differential equations (ODEs). Dynamic systems such as those the RNCRN models are prevalent throughout biology and are critical to many processes such as cellular differentiation and gene expression [35, 36, 37]. As a result, the ability to experimentally construct similar systems which exhibit controllable dynamics has strong potential for applications in therapeutics, diagnostics, and biological regulation.

1.3. Fundamental Research Gap

Despite the ability to use DNA to implement the logic required to build dynamic systems such as the RN-

CRN, a key limitation persists: controlling reaction kinetics in large DNA-based networks. Previous approaches to controlling reaction kinetics have introduced reversible modules for continuous kinetic tuning [38] and explored dissipative and allosteric control strategies [39, 40, 41]. However, these methods often involve sequence-specific constraints or risk introducing unwanted secondary structures. A universal, high-resolution strategy for kinetic control in complex networks remains an open challenge.

The aim of our work is to address this unmet need by introducing a new approach for tunable DNA reaction kinetics via the strategic incorporation of toehold mismatches in DNA strand displacement reactions. By achieving enhanced kinetic control, we can demonstrate that a system with tunable rate constants and precisely programmable temporal behaviours can be successfully constructed. By filling this research gap, we aim to expand the molecular programming toolkit, paving the way for more complex biomolecular circuits with potential applications in synthetic biology, diagnostics, and autonomous nano-machinery.

2. Proposed System Design

2.1. Design Overview & Considerations

With the aim of exploring toehold exchange based kinetic control, we designed the architecture for a primary toehold exchange reaction system. This system, as seen in [Figure 2a](#), consists of a gate complex (G_iO) and invader strand (X) which react to displace the incumbent strand (O) from the gate duplex. To measure the system without interfering with its natural kinetics, we designed a secondary reaction which runs simultaneously to the first: a reporter system. This system consists of the displaced O strand and a complementary DNA duplex which has been chemically modified to have an ATTO 565 fluorophore [42] and associated quencher molecule attached to each of its strands (denoted F & Q). The ATTO 565 fluorophore is a fluorescent molecule that emits light at specific wavelengths when excited within its excitation spectrum. However, when bound next to a quencher molecule the amount of fluorescent light emitted will be significantly reduced.

In the secondary system in [Figure 2b](#), the O strand interacts with this reporter duplex in an additional toehold exchange reaction, displacing the Q strand and resulting in unquenched fluorescence. The reporter therefore provides a means by which to use fluorescent intensity to measure the extent to which the primary system has reacted. Critically, the reporter system eliminates the need for direct fluorescent labelling of the primary system, which could impact the ther-

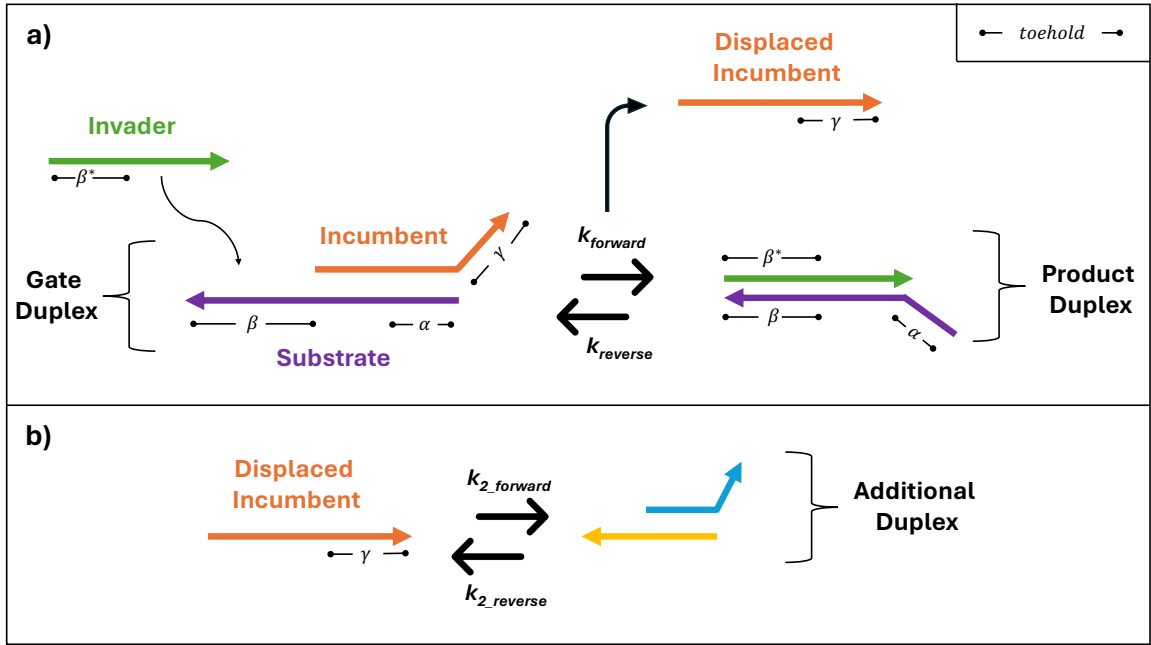


Figure 1: In this and all subsequent figures, directional coloured arrows represent DNA strands. The arrow points from the $5' \rightarrow 3'$ end of the strand and strands are labelled according to their function in the system. Arrows that are arranged parallel (and directly on top of each other) represent strands that are bound into a complex, or a set of multiple bound DNA strands. Toehold regions, indicated in black, are unbound DNA overhangs that act as binding sites for complementary strands. Complementary domains are indicated with an asterisk: i.e. β and β^* . Some toehold regions that are labelled are initially bound within the double stranded portion of a complex and hence do not begin as functional toeholds. These regions may become functional toeholds later in the reaction process, and are noted in their bound form for improved clarity.

(a) Depiction of a standard toehold exchange DNA strand displacement reaction. In this reaction, the invader strand binds to the β toehold region on the substrate – the bottom strand of the gate duplex (a two stranded complex). By reversibly base-pairing with all bases in the toehold, then with additional bases within the region that began as bound within the complex (the branch migration domain), the invader strand slowly displaces the incumbent strand from the gate duplex via a process known as branch migration. Branch migration will only occur when there is sufficient stability at the toehold region to allow the invader strand to compete with the incumbent strand. When this condition is satisfied, the invader displaces the incumbent via the exchange of base pairs in a random walk process. The result is a new duplex consisting of the substrate and the previous invader strand, and the displaced incumbent strand. Note that when the reaction is complete, although the β toehold is no longer functional, or available for binding, the reaction uncovers the α toehold, and maintains the γ toehold. This means there is no reduction in the number of functional toeholds; a key characteristic of toehold exchange making it ideal for systems with cascading reactions. (b) Following the toehold exchange reaction, the displaced incumbent strand can proceed to react in subsequent reactions with other duplexes that have a compatible toehold.

modynamics of the DNA strand binding, and hence the rate constant we are trying to predict [43]. To determine the ideal system architecture, we considered stability of the complexes, orthogonality (lack of unintended interaction between strands), and modularity. Specifically, the following considerations were made:

- Displacement of the Q strand from the reporter duplex: When creating duplexes from single strands – a process known as annealing – it is good practice to hold one strand in excess to ensure most of the other strand is reacted properly. In our case,

when the reporter complex is annealed, we choose the Q strand to be in excess. The Q strand will therefore be designed such that it is orthogonal to all other complexes in the system, reducing the chance that the excess Q triggers a reaction – hence we choose it to be the displaced strand in the secondary reaction. Having Q in excess rather than F also results in a less noisy baseline signal as the only fluorescence contributions will be from blocked fluorophore molecules.

- As shown in Figure 3a, the gate and reporter

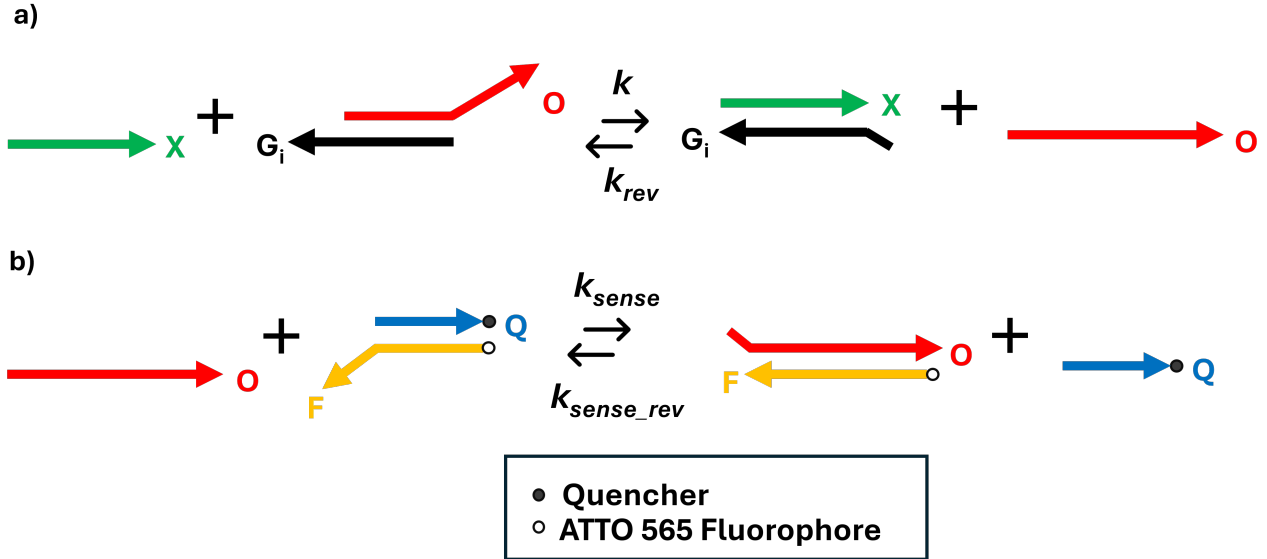


Figure 2: The final design of the full reaction system for tuning and measuring kinetic rate constants of strand displacement reactions. The design consists of two toehold exchange reactions which are set up together and run simultaneously. For the secondary reaction to occur, the preliminary reaction must first execute successfully (a) The primary reaction of interest. In this reaction, the displacement of the O strand is facilitated by the invader, X. The letter k represents the rate constant to be estimated for the system, and hence the kinetic parameter we are aiming to control. k_{rev} , k_{sense} , and k_{sense_rev} correspond to the reverse reaction rate of the primary system and the forward and reverse reaction rates of the reporter system accordingly. (b) The reporter system in which the displaced incumbent strand O from the primary reaction reacts with reporter complex FQ. The result of this secondary reaction is a fluorescent signal produced by unquenched fluorophore molecules that is proportionate to the concentration of the first system that has successfully reacted.

are designed such that one of the complementary pairs ($h-h^*$) begins as “clamped”. This means the h base of the F strand is bound to its complement in the Q strand, and not free for interaction with other strands. This clamped base pair ensures the invader strand (X) cannot easily trigger the reporter system without first releasing O.

- The use of a reporter reaction system is applied as a means to reduce the back-reaction of O with product complex XG_i . By removing free O from solution, we limit the amount of potential “leak” reaction that could occur via back-reaction of O with the reacted gate complex [25].
- Linker regions with sequence TTT are added to the design of the 5' end of the F strand and 3' end of the Q strand. These bases provide a “cushion” of space between the DNA strands and their corresponding fluorophore and quencher molecules, mitigating some of their thermodynamic effects [44].
- All toeholds are designed to be perfectly complementary, with the toehold region of the G_i strand intended to be edited via base pair mismatches in future testing.

- The X and O strands are designed such that they do not form secondary structures such as hairpins in their single strand form. Self-compatibility is avoided to keep single X and O strands from binding to other copies of themselves. This minimizes potential interference with the reactions these strands must initiate (the main and reporter reaction respectively).

The final system architecture based on these considerations is found in Figure 3b.

3. In Silico Simulations

3.1. Reaction System: Sequence Design & Testing

Following the design of the initial architecture, the specific strand sequences were determined. This was done by running a series of multi-tube design ensembles in Python using the NUPACK 4.0.1.12 software [45]. Each tube was set up with desired outputs and “off-targets” to specify which complexes should and should not be present at each stage of the reaction (Figure 4).

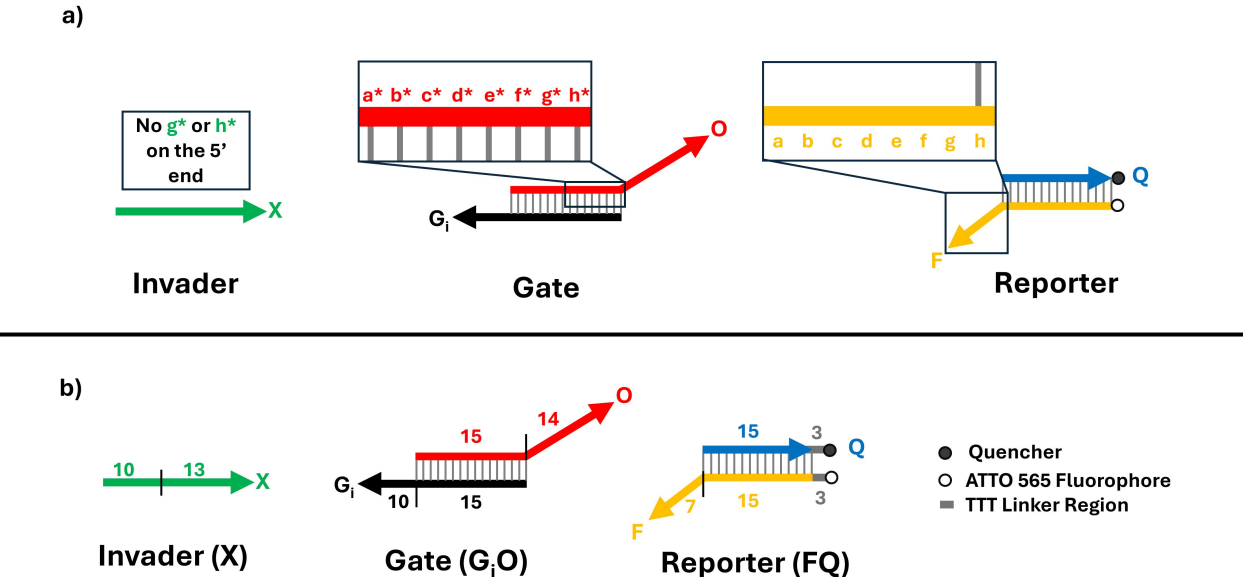


Figure 3: (a) *Clamped-base Design*. As illustrated, the gate and reporter strands are configured such that the $h-h^*$ base pair is initially sequestered or “clamped”. Here the asterisk (*) denotes the complementary domain; for example, h^* is the Watson-Crick complement of domain h . Throughout this schematic, single-letter labels are used in place of actual nucleotides (A, T, C, G) and grey lines linking strands display bonds between complementary base pairs. Initially, the h domain of the reporter strand (F) is bound to its complementary domain on the quencher strand (Q), preventing fluorescence until displacement occurs. Critically, the invader strand does not have either g^* or h^* base pairs on its 3' end. In the context of the clamped base set-up, this ensures that neither the invader, nor the overhang from the O strand, are likely to interact with the F strand toehold and displace Q without the O strand first being fully displaced. (b) Illustration of the finalised structural layout of the DNA reaction system. Number labels indicate the length (in bases) of each domain within the respective strands. The reporter complex includes a fluorophore (ATTO 565) on the F strand and a quencher on the Q strand, each separated from the main portion of the strand by a TTT linker region.

The parameters outlined in Table 1 were then adjusted over the course of six design iterations in which different parameter values were combined to yield distinct systems. The resulting 6 outputs were sorted by defect size (indicative of how closely the design fits the input specifications) and free energy of the end complexes; the initial thought being that a lower free energy indicates higher thermodynamic favourability and more robust systems.

The designs with the lowest free energy and smallest defect size were tested in the webpage-based NUPACK software [47] to determine that no secondary structures formed. For this, the maximum allowable complex size was set to 4 and checks were conducted at different concentrations with particular attention paid to the O and X strands in their single stranded form. The final designs we selected, outlined in Table 2, do not form secondary structures *in silico* at concentrations up to $1 \mu\text{M}$.

3.2. Toehold Mismatch Generation

Following the design of the specific sequences in the main system architecture, attention was shifted to the effect of mismatches within the G_i 10-base toehold. Using Python and NUPACK, 3675 different 10-base toeholds were generated with 1, 2, and 3 mismatches in different locations along the domain [48]. For each of these G_i toeholds, NUPACK was used to obtain the free energy of the structures G_iO and G_iX , and the difference in free energy was taken as the ΔG for the reaction. These free energies were used to calculate a predicted bimolecular rate constant (Appendix B) [25]. The rate constants were plotted in MATLAB with respect to their ΔG values to obtain Figure 5.

3.3. Basic Statistical Analysis of Toehold Distributions

To understand the range of dynamics that could be simulated with our system, a basic statistical analysis of our ΔG values was conducted, as illustrated in

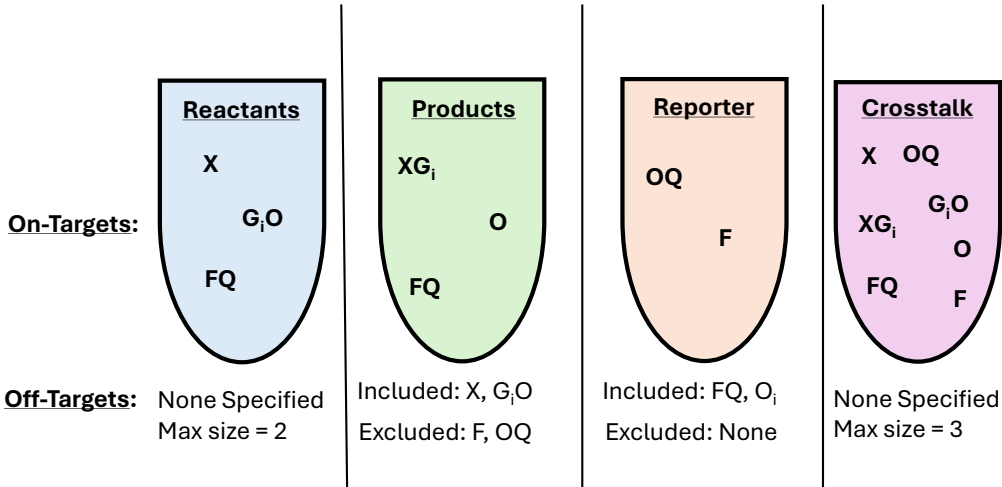


Figure 4: *Schematic of the Multi-Tube Design Ensemble used for sequence validation in NUPACK 4.0.1.12.*
Each ensemble consisted of four test tubes – Reactants, Products, Reporter, and Crosstalk – each with defined on-target complexes (desired outputs) and off-target constraints (undesired or excluded species). Each test tube was set up to simulate a certain stage of the reaction process, with the simulated reactant tube intended to represent the initial setup of the reaction, the products tube the intermediate stage, and the reporter tube the ultimate reaction of the secondary system. The crosstalk tube is included to capture the effect of unplanned interactions between different species that occur over the course of the entire reaction [46]. Species within each test tube graphic depict on-targets for that simulated reaction tube. Information about the off-targets is listed below each tube and contains records of compounds included in the list of undesired species, compounds excluded from the list of undesired species (but still not on-targets), and maximum complex sizes (units: number of strands).

Figure 6. By plotting the probability mass function (PMFs) of the ΔG values obtained for 1, 2, and 3 mismatches, we gain a sense of which ΔG values were most likely to be represented by each number of mismatches; confirming hypotheses that more mismatches lead to more positive ΔG values and therefore less thermodynamically favourable reactions. By plotting the PMFs, we also verify that by using between one and three mismatches, we can obtain the range of ΔG values required to form a complete set of predicted rate constants spanning all experimentally feasible kinetics. Furthermore, the more concentrated peak in probability density in the sets of toeholds with fewer mismatches indicates the interesting feature of this system that fewer mismatches could lead to more robust results. For example, if someone were to use a designed sequence with one mismatch and an error in the placement of the mismatch were to occur, we would expect much less deviation in the resultant ΔG , and hence more similar kinetics, than if there were a similar error in a 3-mismatch sequence. Finally, we note that although these analyses are useful, they are in no way comprehensive. In particular, although all three probability densities are compared directly, the number of possible designs represented by those distributions is not equal: From our simulations, we examine 30 sequence designs with one, 405 with two, and 3240 with three mismatches. Regardless, the analyses provide a good indication of the potential scope of the generated

strand database.

3.4. Final Strand Selection

Once all mismatches had been generated and assessed, the group identified six rate constants with which to examine the experimental scope and accuracy of the predicted dynamics: 1.0×10^1 , 1.0×10^2 , 1.0×10^3 , 1.0×10^4 , 1.0×10^5 , 1.0×10^6 ($M^{-1}s^{-1}$). Toeholds were selected from the database of 3675 designs based on proximity to the desired rate constants and a lack of secondary structures when tested using NUPACK software [47].

The sequences of the selected G_i strands, alongside a depiction of the toehold mismatches can be found in [Table 3](#).

3.5. Simulation Limitations & Discussion

Although these *in silico* design tools and simulation methods proved very useful in design and analysis, there remain a few key limitations.

Parameter	Description	Values Used	Justification
Iteration Number	Number of design iterations performed by NUPACK before returning a potential design	1–5	Used to balance design time and solution quality
Similarity Constraints	Forces portions of the strand domain to match a reference sequence within a specific fractional range; used to constrain sequence composition to include certain percentages of a given nucleotide	45–55% GC content per strand	Ensures thermodynamic stability
Diversity Constraints	Forces a given window of nucleotides to contain a set degree of specified diversity, i.e., for each set of 4 nucleotides must have at least 2 distinct bases	(sequence length = 6, distinct bases = 3) (sequence length = 4, distinct bases = 2)	Reduces repetitive sequences that can lead to unintended secondary structure
Multi-Ensemble Defect Weight	Mechanism to tune the design criteria priorities for different portions of the design ensemble	1–3	Allows weighting of different reaction tubes based on their importance

Table 1: Outline of the key parameters used during DNA strand design in NUPACK [46]. Each parameter is presented with a description of its meaning, the range of values that were applied over the course of the design process, and a rationale for the use of each parameter. Included in the justification column is also information on why the chosen values are useful to the design.

Strand Name	Sequence (5' → 3')
X	GCGCCTAAATCACTCCACTA
O	CACTCCAACTCCACCTCCATCCACCTAC
G _{init}	GTGGAGTTAGGAGTGATTAGGC
F	TTTGTAGGTGGATGGAGGTGGAGTT
Q	CCTCCATCCACCTACTTT

Table 2: Initial strand sequences designed using NUPACK. The strand G_{init} represents the ideal G_i , designed without mismatches.

Strand Name	Sequence (5' → 3')
G_{init}	GTGGAGTTAGGAGTG <u>ATTAGGCGC</u>
G_{1e6}	GTGGAGTTAGGAGTG <u>ATTAGG</u> GTA
G_{1e5}	GTGGAGTTAGGAGTG <u>ATTG</u> GAGCGT
G_{1e4}	GTGGAGTTAGGAGTG <u>ATTG</u> GGACGT
G_{1e3}	GTGGAGTTAGGAGTG <u>GT</u> TTAGG TGT
G_{1e2}	GTGGAGTTAGGAGTG <u>GT</u> TTAGACGT
G_{1e1}	GTGGAGTTAGGAGTG <u>GT</u> TTGGAG GC

Table 3: Strand sequence designs of all gate strands (G_i). The initial G_i strand with no toehold mismatches is denoted as G_{init} . All subsequent strands are denoted with their predicted rate constant as a subscript. For each strand, the toehold region has been underlined and mismatches have been identified in red.

3.5.1. NUPACK & ΔG Calculation

First, the decision to employ NUPACK came with both critical benefits and notable drawbacks. NUPACK was initially selected as an efficient means by which to collect data about a large range of strands and toeholds, including critical ΔG values. However, one drawback of using NUPACK to determine values such as the ΔG is that the reference value used in NUPACK for the calculation of ΔG values is not the same as the standard 1 M reference; consequently, if the offset produced by this difference in reference values is significant, the strand designs we selected and their associated rate constants could all be substantially shifted, as seen in the comparison of Figure 7a & Figure 7b. Initial simulations did not account for this difference in reference value, and this offset could be a source of error in subsequent rate constant calculations. It is also notable that too much importance can not be placed on the sign of the ΔG values obtained when considering the thermodynamic spontaneity of the reaction system, as a positive ΔG value in the NUPACK reference could correspond to a negative ΔG by the standard reference.

3.5.2. Rate Constant Calculations

Further inaccuracy in our simulations may stem from the process used to determine the rate constants [25]. Although the model this process is based on provides a good reference point for order-of-magnitude kinetic

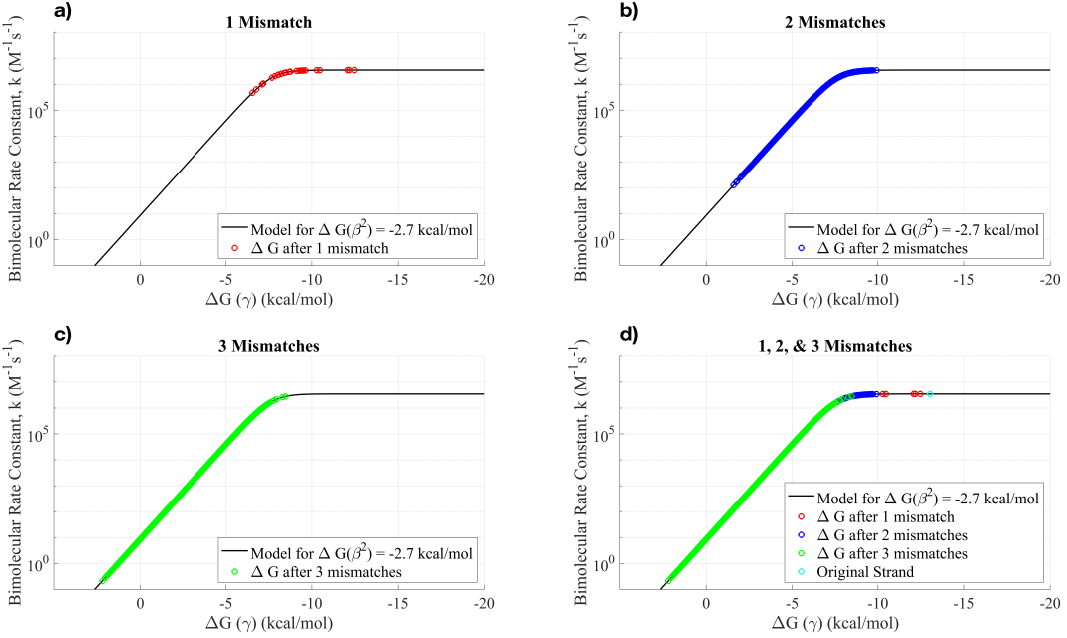


Figure 5: (a) Graphical analysis of the predicted bimolecular rate constants as a function of free energies for strands with a single mismatched base pair. In black, the rate constant for ΔG values from [-20 5] is plotted as predicted by the model outlined in [Appendix B](#) for $\Delta G = -2.7$. The bimolecular rate constants predicted by the model for the ΔG value found via NUPACK for each strand design is plotted in red. The ΔG and model-predicted bimolecular rate constant of the perfectly complementary G_{init} strand is depicted in light blue. Panels (b), (c), and (d) also include the model in black and complementary strand in light blue. In both (b) and (c) the bimolecular rate constants for the ΔG values predicted by NUPACK for each strand design with 2 and 3 mismatches are plotted in blue and green respectively. Panel (d) displays a summary plot of 1, 2, and 3 mismatches overlaid for direct comparison.

estimates, certain assumptions must be noted as potential sources of error. In particular, the model assumes:

- A reaction with intermediate steps can be modelled as a simple bimolecular reaction by neglecting intermediate species.
- The rate at which intermediates begin to form from the initial reactants and the rate at which intermediates begin to form from the final products are equal ($k_{f1} = k_{f2}$ – [Appendix B](#)). It has been demonstrated that k_{f1} , and likely k_{f2} , are in-fact highly sequence dependent and may not be equivalent [25].
- Experimental data that was obtained using a 10 mM magnesium solution is assumed to be equivalent to that obtained using a 1 M sodium solution.
- The value of the rate constants denoting the hybridisation rates of the toeholds to their complements (k_{f1} & k_{f2} – [Appendix B](#)) can be taken from fitted experimental data [25].

- Both the hybridization and branch migration rates used in this model are only good indicators of reaction kinetics beneath a critical concentration threshold which is toehold-dependent.

These assumptions could be a potential source of discrepancy between the theoretically simulated rate constants and their true experimental value. Additionally, although the accuracy of the model for our system is not well understood in the context of these assumptions, the rate constants we obtained were recorded to more than 5 significant figures. Although this level of precision can be reported using such analyses, this resolution is neither accurate nor helpful in predicting the actual dynamics one would expect experimentally.

4. Experimental Verification

Following the completion of the design and *in silico* verification, the reaction system was moved to experimental testing.

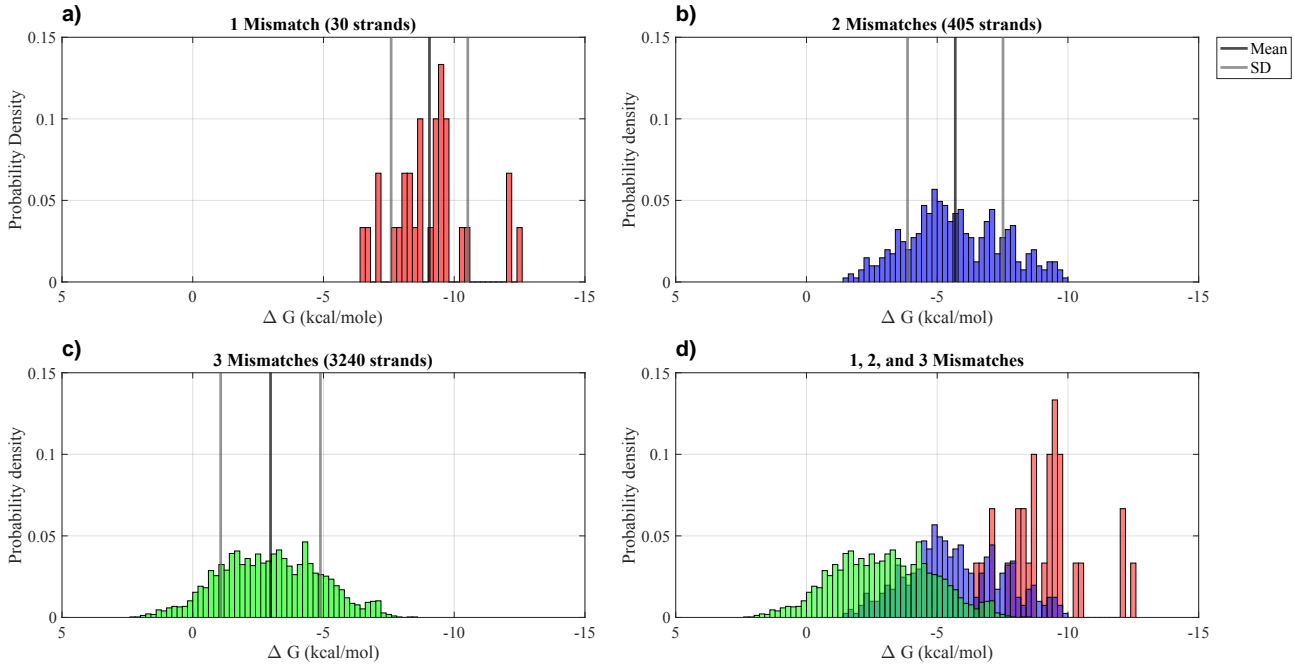


Figure 6: (a) Probability mass function (PMF) of the ΔG values of 30 strands with one toehold mismatch. A black line is plotted to indicate the mean ΔG value and grey lines are plotted to indicate one standard deviation (SD) from the mean in either direction. (b) PMF of the ΔG values of 405 strands with two toehold mismatches. (c) PMF of the ΔG values of 3240 strands with three toehold mismatches. Panels (b) and (c) also display the mean in black, and SD from the mean in grey for the ΔG values of strands with two and three mismatches. (d) Overlaid plot of the PMFs of strands with 1, 2, and 3 mismatches for direct comparison. Full details of how the PMFs were obtained can be found in [Appendix C](#).

4.1. Initial Design - Methods & Materials

To prepare DNA duplexes for experimentation, oligonucleotide strands were annealed using a ThermoFisher ProFlex thermocycler. The complexes were assembled as follows:

- G_iO : G_i and O strands were mixed, with O in 20% excess
- FQ : F and Q strands were mixed, with Q in 20% excess
- FO : F and O strands were mixed, with O in 20% excess

Samples were raised to a temperature of $95^{\circ}C$ and then cooled to $4^{\circ}C$ over 80 minutes to facilitate proper annealing. All DNA oligonucleotides used in this report were synthesised by Integrated DNA Technologies (IDT). Fluorophore labelling was also performed by IDT where applicable.

To ensure the accuracy of the kinetic measurements, preliminary experiments were performed prior to testing of the full system design. These experiments included obtaining a set of calibration curves to link fluorescence values to experimental concentrations ([Ap-](#)

[pendix D.1](#)), characterisation of reporter complex kinetics ([Appendix D.2](#)), and testing for leak reactions in the absence of a displaced incumbent strand ([Appendix D.3](#)). Ultimately, these analyses resulted in the conclusion that no substantial leak reaction occurs and that the reporter complex reacts at a sufficiently fast rate to accurately capture the kinetics of the primary system. The full analysis of these preliminary experiments can be found in [Appendix D](#). We were then ready to proceed to testing our main reaction system.

To check for tuneable system kinetics, all G_i strands were individually tested as part of the full reaction system. For each G_i variant, experiments were performed in triplicates to reduce the effect of random error. As part of each reaction experiment, positive and negative controls were also prepared and measured. Positive control wells contained known concentrations of pre-annealed FO at 5, 10, 15 and 20 nM concentrations and were measured in triplicates. Negative controls included wells containing buffer and buffer mixed with FQ , enabling the determination of baseline fluorescence.

All fluorescence measurements were carried out using a POLARstar microplate reader. The reader was configured with an excitation wavelength of 550 nm and an emission wavelength of 590 nm, matching the spectral

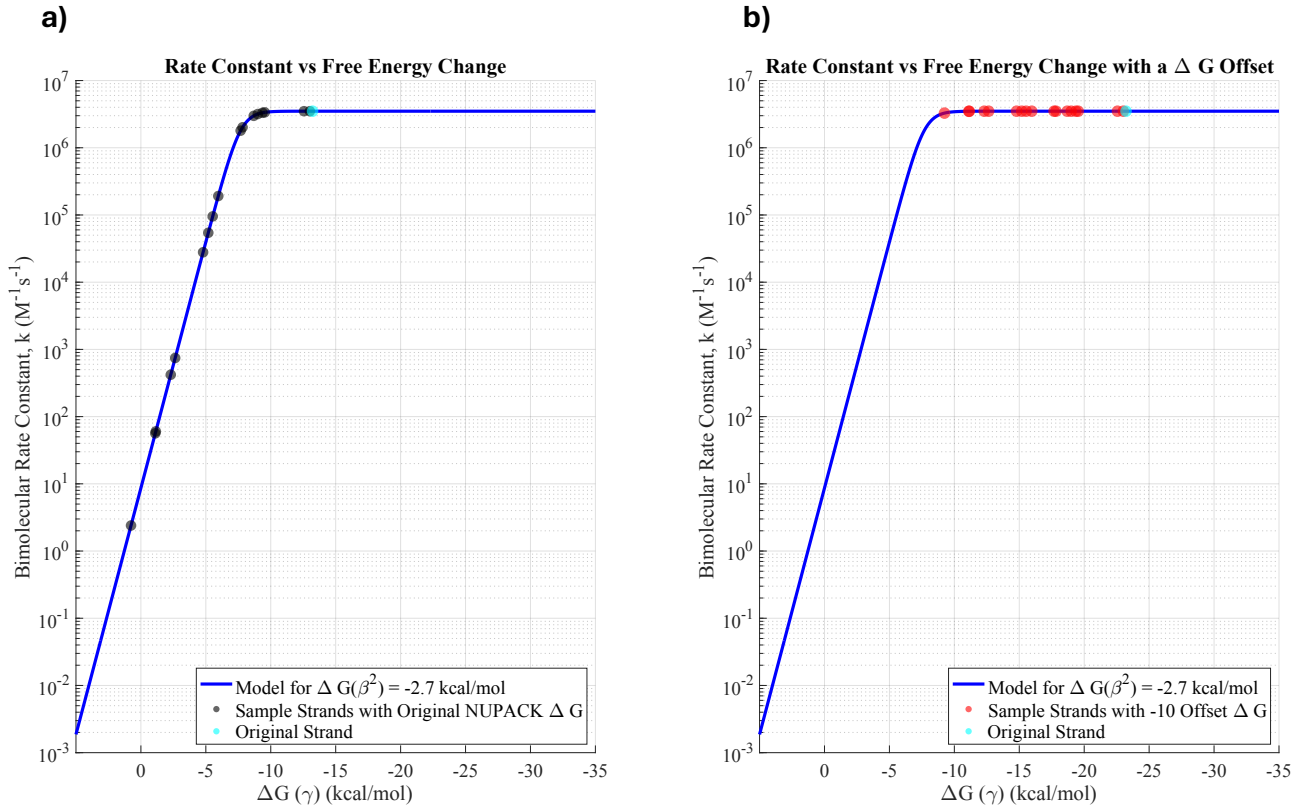


Figure 7: (a) Rate constants plotted against the free energy change (ΔG) for 10 unique strand designs using ΔG values computed by NUPACK. (b) The same 10 strand designs shown with an arbitrary -10 kcal/mol offset applied to ΔG . The applied offset significantly shifts the corresponding rate constants, highlighting the sensitivity of rate constant predictions of the chosen model [25] to the ΔG values used. Although these strand designs and offset are not specific to our experiments, they demonstrate how an artificial shift in the ΔG values as a result of using NUPACK without adjustment could result in a significant mismatch in the observed experimental and theoretical rate constants.

characteristics of the ATTO 565 fluorophore [42]. Fluorescent intensity was continuously monitored providing quantitative data for analysis of reaction kinetics. The full procedure used to assess the G_i strands can be found in P9.1.

4.2. Initial Design - Results

Relying on our assumption that the reporter complex is reacting at sufficient speed to capture the true kinetics of the primary reaction system, we successfully measured the rate constants of the system for G_{init} , G_{1e6} , G_{1e4} , G_{1e3} , and G_{1e2} , as seen in Table 4. Unfortunately, we encountered issues with the fluorescence measurements of G_{1e5} and G_{1e1} due to equipment malfunction and experimental errors; these experiments were not redone due to time constraints.

For every well measured in each reaction system, we fitted the acquired data using the ODE specified in F4.1 as illustrated in Figure 9 for G_{1e2} . The fitted parameters of the ODE (rate constant and final concentration)

were noted for each well and averaged across the wells of each distinct G_i strand to obtain the final values recorded in Table 4 and Table 5. To quantify the accuracy of the fit, the sample standard deviation (σ_k) for each G_i strand was recorded. Furthermore, the average Root Mean Square Error (RMSE) of the fitted rate constants was calculated for each of the triplicate measurements and averaged to obtain the overall RMSE for that G_i strand. The results of the standard deviation and RMSE analysis can be found in Table 4. It is of note that the RMSE values calculated for each triplicate were roughly equal across concentrations. However, considering that concentrations varied from 2-10 nM, this means that at smaller concentrations the error comprised a larger percent of the reported value, leading to the conclusion that concentrations closer to 10 nM likely yielded more accurate measurements of the experimental rate constant.

Gate	$k (\times 10^6 \text{ Ms}^{-1})$		RMSE (nM)
	\bar{k}	σ_k	
G_{init}	0.88	0.31	0.1735
G_{1e6}	3.17	0.72	0.1294
G_{1e4}	3.26	0.96	0.1322
G_{1e3}	1.59	0.55	0.1482
G_{1e2}	1.08	0.38	0.1339

Table 4: Summary of fitted kinetic parameters for each gate strand. For each gate, the average rate constant \bar{k} was obtained by fitting the reaction model to experimental data and averaging over the rate constants determined via fitting individual curves for each of three triplicate measurements. The standard deviation σ_k quantifies variability in the rate constant across triplicate measurements. The Root Mean Square Error (RMSE) indicates the average fitting error of the model to experimental data.

Gate	$[X_T] (\text{nM})$				
	X_1	X_2	X_3	X_4	X_5
G_{init}	1.272	3.095	5.439	8.005	9.575
G_{1e6}	1.637	3.147	5.017	6.833	7.644
G_{1e4}	1.403	3.026	4.690	6.273	6.665
G_{1e3}	0.910	1.116	2.747	4.402	5.791
G_{1e2}	0.676	1.789	3.294	4.901	6.422

Table 5: Fitted parameter $[X_T]$ averaged over each triplicate and recorded for each well. The parameter $[X_T]$ represents the final concentration of G_iX in our system i.e. the total concentration of invader that has displaced the incumbent strand at steady state. The wells X_1, X_2, X_3, X_4 and X_5 were intended to contain approximately 2 nM, 4 nM, 6 nM, 8 nM and 10 nM of the invader strand respectively

4.3. Discussion

4.3.1. Key Observations

Observing these statistics and the kinetic curves yielded by our system analysis, three key things are immediately apparent:

1. All rate constants calculated for each G_i strand (Table 4) are in the 1×10^6 order of magnitude range.
2. Prior to the nuking step (defined in P6), full conversion of reactant strands into the intended product is not achieved in the well injected with 10 nm of invader. Nuking pushes the reaction to the product side resulting in a higher end concentration.

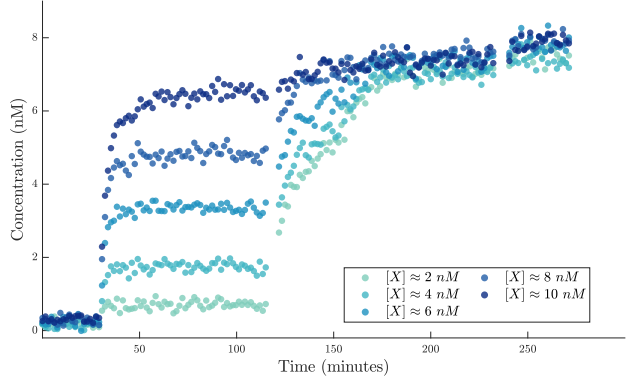


Figure 8: Concentration of FO during one triplicate measurement during the experimental verification of G_{1e2} . Concentrations of the invader strand X that were injected into the experimental wells range from 2 nM to 10 nM in steps of 2 nM and are indicated by colour. In contrast to Figure 9, this dataset does not include any fitting to the ODE model, and is inclusive of both nuking steps where the system is saturated with high concentrations of the invader strand of both the primary and reporter systems (X and O). The nuking step is apparent in the abrupt increase in concentration after the initial reaction reaches a steady state at an approximate time of 120 minutes. Notably, the sample injected with 10 nM, which would ideally result in nearly full conversion of gate strands to product species, still has a visible increase as a result of the nuking step.

3. All final concentration values are lower than expected, with values of X_1, X_2, X_3, X_4 , and X_5 reaching below their optimally expected values of 2, 4, 6, 8, and 10 nM respectively (Table 5).

The consistency observed in the rate constants deviates substantially from the order of magnitude differences expected between each of the gate designs tested. This deviation suggests one of three things: that it may not be possible to achieve our desired range of kinetics using toehold mismatches; that errors in our experimental procedures resulted in a misrepresentation of the true kinetics; or that errors in our *in silico* simulations resulted in discrepancies from the true experimental values. As discussed in subsubsection 4.3.2, we believe the most likely explanation is that simulation errors resulted in a difference between our expected and obtained values.

Regarding the incomplete conversion of reactants to products prior to nuking (see Figure 8), a thermodynamic drive is required to result in such a conversion. For example, the presence of longer, more GC-rich do-

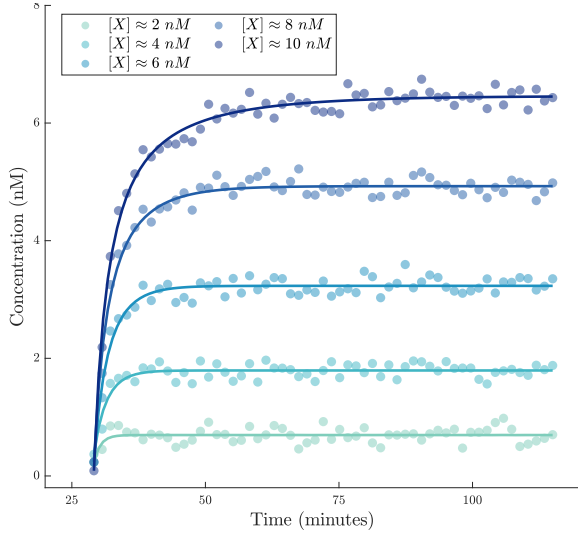


Figure 9: Concentration of FO during one triplicate measurement during experimental verification of G_{1e2} . Concentrations of the invader strand X that were injected into the experimental wells range from 2 nM to 10 nM in steps of 2 nM and are indicated by colour. Fitted kinetic curves are applied to the data for each concentration and used to calculate the experimental rate constant for each concentration. These rate constants were used as part of the average rate constant calculated for this reaction and found in [Table 4](#).

mains in the product species would shift the thermodynamic equilibrium of the reaction to more heavily favour the product species. It is possible that sufficient thermodynamic drive from such factors is not present in our system prior to saturation of the system with the nuking agents. However, it is worth noting that for our system we would expect the presence of mismatches to improve the forward thermodynamic drive [\[49\]](#).

Finally, as far as the lower final concentration values observed across each gate strand analysis, two key points are of interest: why we see a reduction in concentration, and how consistent this reduction is across different gate analyses. It is possible that some reduction in concentration is a consequence of the choice to anneal our complexes with excess O as described in [subsection 4.1](#). Because we begin our reaction with an excess of O in the microplate wells, we expect the O strand to begin triggering the reporter system prior to reaction initiation by the invader strand. This is accounted for in our data analysis process in [F3](#). However, what we do not account for is the fact that there is an effectively lower initial concentration of FQ available to interact with displaced O strands once the primary reaction system has been triggered. To test this source of error, the use of a higher initial reporter complex (FQ) concentration could be assessed.

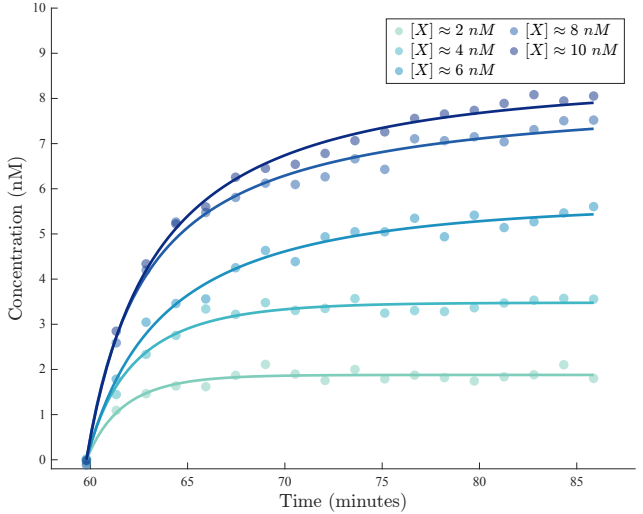


Figure 10: Concentration of FO during one triplicate measurement during experimental verification of G_{init} . Concentrations of the invader strand X that were injected into the experimental wells range from 2 nM to 10 nM in steps of 2 nM and are indicated by colour. Fitted kinetic curves are applied to the data for each concentration and used to calculate the experimental rate constant for each concentration. These rate constants were used as part of the average rate constant calculated for this reaction and found in [Table 4](#). Note that the final concentrations in this reaction are not evenly spaced in the step-wise manner we would expect. Additionally, the steepness of the initial kinetic region of the different concentrations all visibly vary, with the 8 and 10 nM samples following a nearly identical trajectory until approximately minute 65 .

Further to the overall reduction in final concentrations, the observed decrease in concentrations is also inconsistent across the gates that were tested (with G_{init} having a final X_5 value of 9.575 nM and G_{1e3} having a final X_5 of 5.791 – both of which should have been 10 nM). This discrepancy could be partially attributed to errors in the pipetting and annealing processes, but further experimentation would need to be conducted to verify whether this is likely to be the case.

Beyond these three systematic observations, we also note that anomalous results were observed for the G_{init} strand, where the measured reaction kinetics deviated from our theoretical predictions ([Figure 10](#)). The cause of this behaviour remains unclear but can likely be attributed to error during experimental setup.

4.3.2. Experimental Outcome

Overall, despite these discrepancies from our theoretical predictions, we note that for the strands that were tested successfully, the data collected was well-fit by the ODE model used to describe the bimolecular reaction ([Equation F4.1](#)). This indicates that the reaction system is likely operating as intended and the experimental protocol is yielding consistent results. These observations imply that the discrepancies identified in [subsubsection 4.3.1](#) are likely not a result of issues with the experimental setup, and we therefore consider that our simulations are probably the main source of deviation from our theoretical rate constants.

Consequently, we determine that although the experimental rates of the selected strand designs are not significantly different, the overall system design does function as intended. However, to understand how to successfully achieve a range of system kinetics, our initial simulations had to be re-explored and new experimental testing executed. To do this, the biggest sources of error in our *in silico* simulations was first identified.

5. Second Design Iteration & Future Plans

5.1. Problem Identification & Designing New Strands

In examining our *in silico* simulations, two potential causes for the experimental inconsistencies were identified.

First, mismatches within the three bases adjacent to the branch migration domain of the toehold may have influenced the reaction kinetics. Such mismatches could destabilise the double-stranded complex, increasing its susceptibility to strand displacement and therefore, increasing the reaction rate. Alternatively, such mismatches could have an impact on the stability of the hybridisation of intermediates within the toehold exchange reaction which could also influence the kinetics of the system.

Second, a systematic offset in the calculated rate constants may have arisen from differences in the ΔG values used in NUPACK simulations and the standard values assumed in our rate constant calculations, as outlined in [subsubsection 3.5.1](#). This is illustrated in [Figure 7](#), and could explain why our experimental results have very similar kinetic profiles despite their initial range of theoretical values.

To isolate what may be causing the discrepancy, we

chose to focus on the first potential issue: mismatches near the branch migration domain. To address this source of error, new strands were selected from the original database ([subsection 3.2](#)) to target reaction rates of 10^1 , 10^2 , and $10^3 \text{ M}^{-1}\text{s}^{-1}$. Strands were screened to avoid secondary structures and selected such that they contained no mismatches within the first three bases upstream of the branch migration domain. This additional consideration aimed to reduce the thermodynamic impacts of unforeseen duplex instability.

5.2. Experimental Verification of New Strands

Gate	$k (\text{M}^{-1}\text{s}^{-1})$	RMSE (nM)
$\mathbf{G}_{4\mathbf{e}1^*}$	4.85×10^4	0.1898
$\mathbf{G}_{1\mathbf{e}2^*}$	4.12×10^4	0.1718
$\mathbf{G}_{1\mathbf{e}3^*}$	6.60×10^5	0.1957

Table 6: *Fitted rate constants for each of the redesigned gate strands and the RMSE of the fitted ODE. Each rate constant is only measured from fitted data obtained with an injected invader concentration of 10 nM. The * in the subscript of each G_i indicates a strand that has been selected as part of the second design iteration.*

The newly designed strands were then evaluated in the full reaction system using the same protocols as in the original system testing. The corresponding results are summarised in [Table 6](#), with raw experimental data shown in [Figure 11](#) demonstrating a strong fit between the measured values and the fitted kinetic curves. Among the concentrations tested, only the reactions involving 10 nM of the invader strand yielded results that closely matched the expected kinetic behaviour. For all other concentrations, the data was insufficient to generate a fitted curve per the data analysis protocol ([P10.1](#)). As a result, the data from these concentrations could not be used to extract meaningful rate constants. The reason for this remains unclear but could potentially be due to incomplete initiation of the reaction or pipetting errors when preparing the well plate.

Despite these variations, the reactions involving 10 nM of the invader strand produced rate constants that were consistent in relative magnitude with our simulations (i.e. for strands with a predicted order of magnitude difference between their rate constants, an order of magnitude difference was observed). However, the absolute values remained offset from those predicted by NUPACK, with all reactions still occurring at a faster rate than anticipated. Additionally, the difference in value of the rate constants of the new strands and the

original strands (which did not have mismatches near the branch migration domain) is still not as large as expected. This suggests a remaining systematic discrepancy and will need to be further explored.

Notably, the data supports the hypothesis that avoiding mismatches within the first three nucleotides adjacent to the branch migration domain improves the predictability of rate constants. However, the continued offset in the observed rate constants compared to the predicted values suggests that additional factors, such as the difference in thermodynamic parameters used by NUPACK, may also play a significant role.

Regardless, these results expand the observed range of rate constants and highlight the sensitivity of strand displacement kinetics to changing the position of mismatches in the toehold domain.

5.2.1. Further Investigation

Future work will involve repeating the experiments for the new strands, using the full range of invader concentrations. This will allow the formation of more complete datasets across a wider range of conditions. Further investigation into the source of the ΔG discrepancy between NUPACK predictions and experimentally derived values is also planned with the goal of identifying whether a systematic correction can be applied. In addition, expanding the toehold strand library through the experimental testing of new sequences will expand the scope of our experimentally-verified database. Further to this, we aim to make the results of our work more widely accessible. This is where an interface such as our web-based design tool will be critical.

6. Implementation of a Web-Based Design Tool

6.1. Motivation & Walk-Through

With the goal of making our experimentally verified designs accessible to those creating DNA reaction systems, our website aims to provide an interface for efficient kinetic-based strand selection.

The following section provides an overview of our proposed website highlighting the key inputs, outputs, and background processes. A summary of the website architecture is shown in [Figure 12](#).

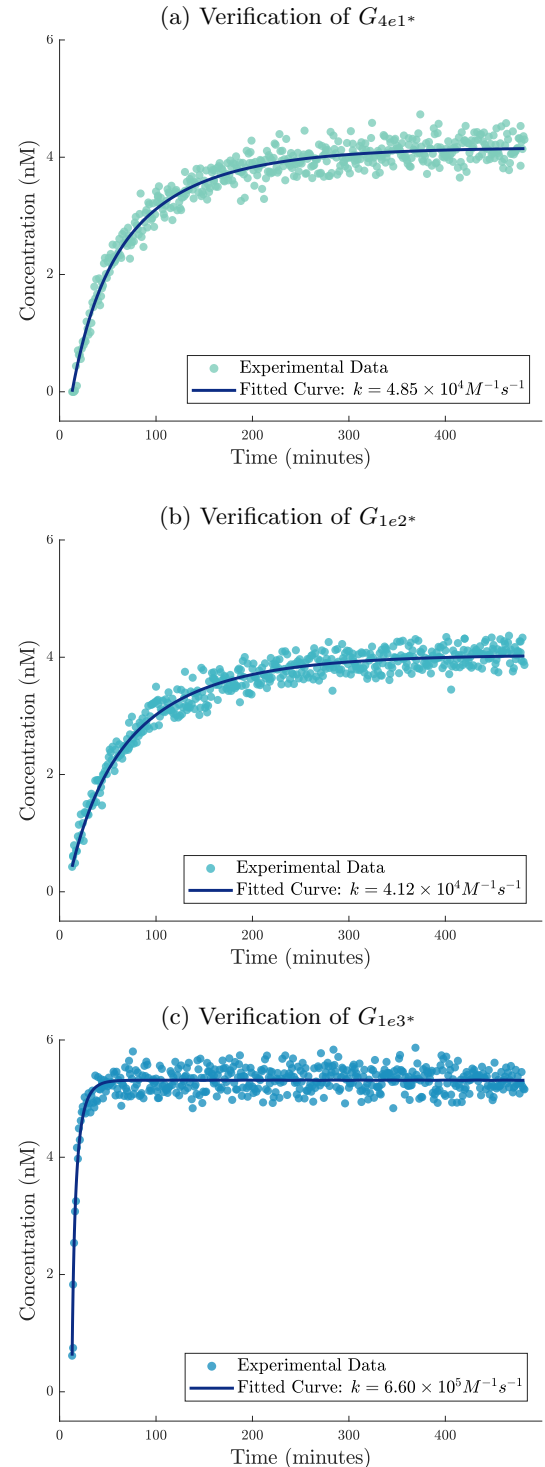


Figure 11: Concentration of FO during verification of three new strands: (a) G_{4e1^*} , (b) G_{1e2^*} , and (c) G_{1e3^*} . Each panel shows the reaction when 10nM of the invader strand X is injected. The fitted curves were used to estimate the rate constants discussed in [Table 6](#).

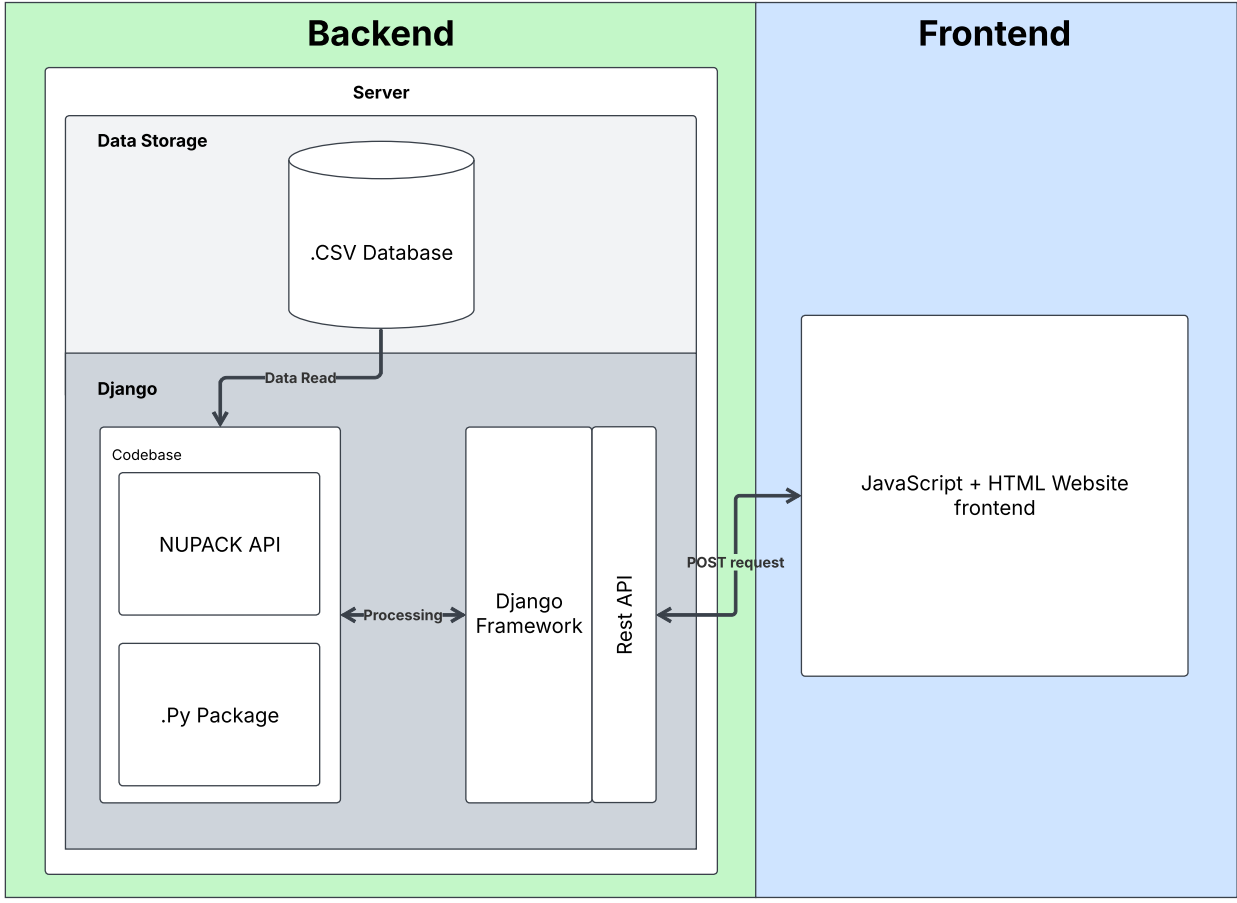


Figure 12: *Diagram outlining the website architecture. The frontend accepts a user-defined rate constant and sends a POST request to the backend. The backend processes the request using internal Python packages and the NUPACK API, retrieving data from a .CSV database. The selected sequence, corresponding rate constant, and analysis results are returned to the frontend for display.*

6.1.1. Step 1: User Input

Upon accessing the web interface (frontend), users are presented with a prompt to enter a desired strand displacement rate constant as shown in Figure 13a. This rate constant defines the kinetic behaviour the user wishes to achieve. While the current web tool accepts only a single numeric input, future iterations may include advanced options such as toehold length, GC nucleotide content, buffering conditions and temperature-dependence.

Once the user submits a rate constant, the system processes the request and identifies a suitable toehold sequence. These implementation details are documented in Appendix E for readers interested in the computational workflow.

6.1.2. Step 2: Backend Processing & NUPACK Integration

Once a match is identified, the tool performs a secondary structure analysis using NUPACK to screen for structural motifs that could hinder strand displacement: hairpins, internal loops, or self-complementary binding regions. The tool queries via the NUPACK API for thermodynamic parameters including the minimum free energy (MFE) and predicted free energy change (ΔG) to ensure the candidate sequence is both stable and functionally reliable [47, 50]. Details of this process are available in Appendix E.

6.1.3. Step 3: Output and User Feedback

Once processing is complete, the backend sends a JSON response containing the selected toehold sequence, its matched rate constant, the NUPACK screening result, and a visual strand representation.

- (a) UI design prior to feedback from potential web-tool users.

DYNAMICS BY DESIGN

- (b) UI following implementation of input from potential web-tool users. The UI is still under development and will be updated again after further feedback from users.

DYNAMICS BY DESIGN

Figure 13: Frontend User Interface (UI) design of the web-based tool.

The frontend presents this clearly, displaying the sequence, a strand diagram, and a pass/fail message as shown in Figure 13b. This allows users to quickly assess the suitability of the returned toehold and understand the basis of its selection.

7. Conclusion

The primary objective of our work has largely been met: we have designed a novel approach for the control of DNA toehold reaction kinetics; constructed a working database of strand sequences with diverse toehold mismatch placement; experimentally validated a subset of our theoretical database; and initiated the development of a platform to allow researchers to use our

system to incorporate kinetic control into their molecular designs. In doing so, we have presented a new toolkit for programmable control over DNA reaction kinetics; the successful implementation of which can yield predictable and scalable behaviours across a variety of strand displacement-based systems.

Although our system itself still requires further development and analysis, our experimental work has already begun to expand the number of well-characterised kinetic strand designs available for research use and application.

Ultimately, this work lays a foundation for broader implementation of kinetic control in molecular programming, providing a means for the implementation of more sophisticated dynamic applications across synthetic biology and biomolecular engineering.

8. Supporting Information

Supplemental information including our Experimental Procedure (P6) and Data Processing Protocol (P10.1) can be found as additional files appended to the end of this document. A complete repository of all code files used in the theoretical simulations, data analysis, and website development is publicly available and can be found [here](#).

9. Acknowledgements

We thank our supervisor Dr. Thomas Ouldridge for all his guidance and support throughout the duration of this project. We thank Alexander Dack for his reading of this report, support in understanding the RNCRN, assistance conducting theoretical simulations and input into the website design. We thank Križan Jurinović for his reading of this report, support using NUPACK, and guidance during the experimental verification of the designs. We are also grateful for Križan Jurinović's instruction regarding suitable data analysis algorithms focussed on minimising the effects of experimental errors. We thank Sing Ming Chan for his input when troubleshooting the outcomes of the first round of experimental results and support during the full experimental verification of the design. We thank the remainder of the Ouldridge research group for the various support they showed this project throughout its duration both in and out of the lab.

10. Generative AI - Statement of Acknowledgement

Although this document does not include content directly created using generative AI, we acknowledge the use of ChatGPT 3.5 (OpenAI, <https://chat.openai.com/>) as an assistive tool in the following tasks:

- De-bugging of small sections of MATLAB and Python code written by the authors.
- LATEX formatting and adjustment of Table parameters in the creation of this report document.

We confirm that no content generated by AI has been presented as our own work.

References

- [1] Winfree E, Liu F, Wenzler L, Seeman N. Design and self-assembly of two-dimensional DNA crystals. *Nature*. 1998;394(6693):539-44.
- [2] He Y, Ye T, Su M, Zhang C, Ribbe A, Jiang W, et al. Hierarchical self-assembly of DNA into symmetric supramolecular polyhedra. *Nature*. 2008;452(7184):198-201.
- [3] Rothemund P. Folding DNA to create nanoscale shapes and patterns. *Nature*. 2006;440(7082):297-302.
- [4] Seelig G, Soloveichik D, Zhang DY, Winfree E. Autonomous molecular cascades for evaluation of logic functions. *Science*. 2006;314(5805):1585-8.
- [5] Yin P, Choi H, Calvert C, Pierce N. Programming biomolecular self-assembly pathways. *Nature*. 2008;451(7176).
- [6] Green S, Bath J, Turberfield A. Coordinated chemomechanical cycles: A mechanism for autonomous molecular motion. *Physical Review Letters*. 2008;101(23).
- [7] Dirks R, Pierce N. Triggered amplification by hybridization chain reaction. *Proceedings of the National Academy of Sciences of the United States of America*. 2004;101(43).
- [8] Yurke B, Turberfield A, Mills A, Simmel F, Neumann J. A DNA-fuelled molecular machine made of DNA. *Nature*. 2000;406(6796).
- [9] Zhang DY, Turberfield AJ, Yurke B, Winfree E. Engineering entropy-driven reactions and networks catalyzed by DNA. *Science*. 2007;318(5853):1121-5.
- [10] Rothemund PW. Self-assembly of DNA into nanoscale three-dimensional shapes. *Nature*. 2006;440(7082):297-302.
- [11] Wickham SFJ, Endo M, Katsuda Y, Hidaka K, Bath J, Sugiyama H, et al. A DNA-based molecular motor that can navigate a network of tracks. *Nature Nanotechnology*. 2012;7(3):169-73.
- [12] Gu H, Chao J, Xiao SJ, Seeman NC. A proximity-based programmable DNA nanoscale assembly line. *Nature*. 2010;465(7295):202-5.
- [13] Seelig G, Soloveichik D, Zhang D, Winfree E. Enzyme-free nucleic acid logic circuits. *Science*. 2006;314(5805).
- [14] Yin F, Wang F, Fan C, Zuo X, Li Q. Biosensors

- based on DNA logic gates. *VIEW*. 2021;2(2).
- [15] Bardales A, Smirnov V, Taylor K, Kolpashchikov D. DNA Logic Gates Integrated on DNA Substrates in Molecular Computing. *ChemBioChem*. 2024;25(8).
- [16] Okamoto A, Tanaka K, Saito I. DNA logic gates. *Journal of the American Chemical Society*. 2004;126(30).
- [17] Lee JB, Campolongo MJ, Kahn JS, Roh YH, Hartman MR, Luo D. DNA-based nanostructures for molecular sensing. *Nanoscale*. 2010;2(10):1880-94.
- [18] Dirks RM, Bois JS, Schaeffer JM, Winfree E, Pierce NA. Thermodynamic analysis of interacting nucleic acid strands. *SIAM Review*. 2007;49(1):65-88.
- [19] Zuker M. Mfold web server for nucleic acid folding and hybridization prediction. *Nucleic Acids Research*. 2003;31(13):3406-15.
- [20] Santa Lucia Jr J, Hicks D. The thermodynamics of DNA structural motifs. *Annual Review of Biophysics and Biomolecular Structure*. 2004;33:415-40.
- [21] Bommarito S, Peyret N, Santa Lucia Jr J. Thermodynamic parameters for DNA sequences with dangling ends. *Nucleic Acids Research*. 2000;28(9):1929-34.
- [22] Srinivas N, Parkin J, Seelig G, Winfree E, Soloveichik D. Enzyme-free nucleic acid dynamical systems. *Science*. 2017;358(6369).
- [23] Park SY, Lytton-Jean AKR, Lee B, Weigand S, Schatz GC, Mirkin CA. DNA-programmable nanoparticle crystallization. *Nature*. 2008;451(7178):553-6.
- [24] Machinek RRF, Ouldridge TE, Haley NEC, Bath J, Turberfield AJ. Programmable energy landscapes for kinetic control of DNA strand displacement. *Nature Communications*. 2014;5(1):5324.
- [25] Zhang DY, Winfree E. Control of DNA strand displacement kinetics using toehold exchange. *Journal of the American Chemical Society*. 2009;131(47):17303-14.
- [26] Qian L, Winfree E. Scaling up digital circuit computation with DNA strand displacement cascades. *Science*. 2011;332(6034):1196-201.
- [27] Douglas SM, Bachelet I, Church GM. A Logic-Gated Nanorobot for Targeted Transport of Molecular Payloads. *Science*. 2012;335(6070):831-4.
- [28] Muscat RA, Bath J, Turberfield AJ. Small Molecule Signals that Direct the Route of a Molecular Cargo. *Small*. 2012;8(23):3593-7.
- [29] Lund K, Manzo AJ, Dabby N, Michelotti N, Johnson-Buck A, Nangreave J, et al. Molecular robots guided by prescriptive landscapes. *Nature*. 2010;465(7295):206-10.
- [30] Cherry KM, Qian L. Scaling up molecular pattern recognition with DNA-based winner-take-all neural networks. *Nature*. 2018;559(7714):370-6.
- [31] Qian L, Winfree E, Bruck J. Neural network computation with DNA strand displacement cascades. *Nature*. 2011;475(7356):368-72.
- [32] Soloveichik D, Cook M, Winfree E, Bruck J. Computation with finite stochastic chemical reaction networks. *Natural Computing*. 2008;7(4):615-33.
- [33] Okumura S, Gines G, Lobato-Dauzier N, Ladoux B, Estevez-Torres A. Nonlinear decision-making with enzymatic neural networks. *Nature*. 2022;610(7930):496-501.
- [34] Dack A, Qureshi B, Ouldridge TE, Plesa T. Recurrent neural chemical reaction networks that approximate arbitrary dynamics. *Nature Communications*. 2021;12(1):5678.
- [35] Xiong W, Ferrell JE. A positive-feedback-based bistable 'memory module' that governs a cell fate decision. *Nature*. 2003;426(6965):460-5.
- [36] Hardin PE, Hall JC, Rosbash M. Feedback of the *Drosophila* period gene product on circadian cycling of its messenger RNA levels. *Nature*. 1990;343(6258):536-40.
- [37] Heltberg ML, Krishna S, Jensen MH. On chaotic dynamics in transcription factors and the associated effects in differential gene regulation. *Nature Communications*. 2019;10(1).
- [38] Wu L, Wang GA, Li F. Plug-and-Play Module for Reversible and Continuous Control of DNA Strand Displacement Kinetics. *Journal of the American Chemical Society*. 2024;146(10):6516-21.
- [39] Del Gross E, Amodio A, Ragazzon G, Prins LJ, Ricci F. Dissipative Control over the Toehold-Mediated DNA Strand Displacement Reaction. *Angewandte Chemie International Edition*. 2022;61(30):e202201929.

- [40] Yang X, Tang Y, Traynor SM, Li F. Regulation of DNA strand displacement using an allosteric DNA toehold. *Journal of the American Chemical Society*. 2016;138(43):14076-82.
- [41] Lysne D, Hachigian T, Thachuk C, Lee J, Graugnard E. Leveraging steric moieties for kinetic control of DNA strand displacement reactions. *Journal of the American Chemical Society*. 2023;145(30):16580-7.
- [42] ATTO-TEC. Atto 565; 2021. Accessed 8 April, 2025. Available from: <https://www.atto-tec.com/ATTO-565.html?language=de>.
- [43] Marras S, Kramer F, Tyagi S. Efficiencies of fluorescence resonance energy transfer and contact-mediated quenching in oligonucleotide probes. *Nucleic Acids Research*. 2002;30(21):e122.
- [44] Moreira B, You Y, Behlke M, Owczarzy R. Effects of fluorescent dyes, quenchers, and dangling ends on DNA duplex stability. *Biochem Biophys Res Commun*. 2005;327(2):473-84.
- [45] Wolfe BR, Porubsky NJ, Zadeh JN, Dirks RM, Pierce NA. Constrained multistate sequence design for nucleic acid reaction pathway engineering. *Journal of the American Chemical Society*. 2017;139:3134-44.
- [46] NUPACK Developers. NUPACK User Manual; 2025. Last accessed 14 April, 2025. Available from: <https://docs.nupack.org>.
- [47] Zadeh JN, Steenberg CD, Bois JS, Wolfe BR, Pierce MB, Khan AR, et al. NUPACK: Analysis and design of nucleic acid systems. *Journal of Computational Chemistry*. 2011;32:170-3.
- [48] Jurinović K. MismatchGeneration.py; 2024. Unpublished.
- [49] Haley NEC, Ouldridge TE, Mullor Ruiz I, Geraldini A, Louis AA, Bath J, et al. Design of hidden thermodynamic driving for non-equilibrium systems via mismatch elimination during DNA strand displacement. *Nature Communications*. 2020;11(1):1-11.
- [50] Dirks RM, Pierce NA. An algorithm for computing nucleic acid base-pairing probabilities including pseudoknots. *Journal of Computational Chemistry*. 2004;25(10):1295-304.
- [51] McKinney W. Python for Data Analysis. O'Reilly Media; 2017.
- [52] Christie T. Django REST Framework - Official Documentation; n.d. Accessed 14 April 2025. Available from: <https://www.djangoproject-rest-framework.org>.
- [53] Richardson L, Ruby S. RESTful Web Services. O'Reilly Media; 2007.
- [54] Amazon Web Services. What is Amazon EC2?; n.d. Accessed 14 April 2025. Available from: <https://aws.amazon.com/ec2>.
- [55] Jurinović K. Standard Procedure for Strand Displacement Systems; 2024. Unpublished.

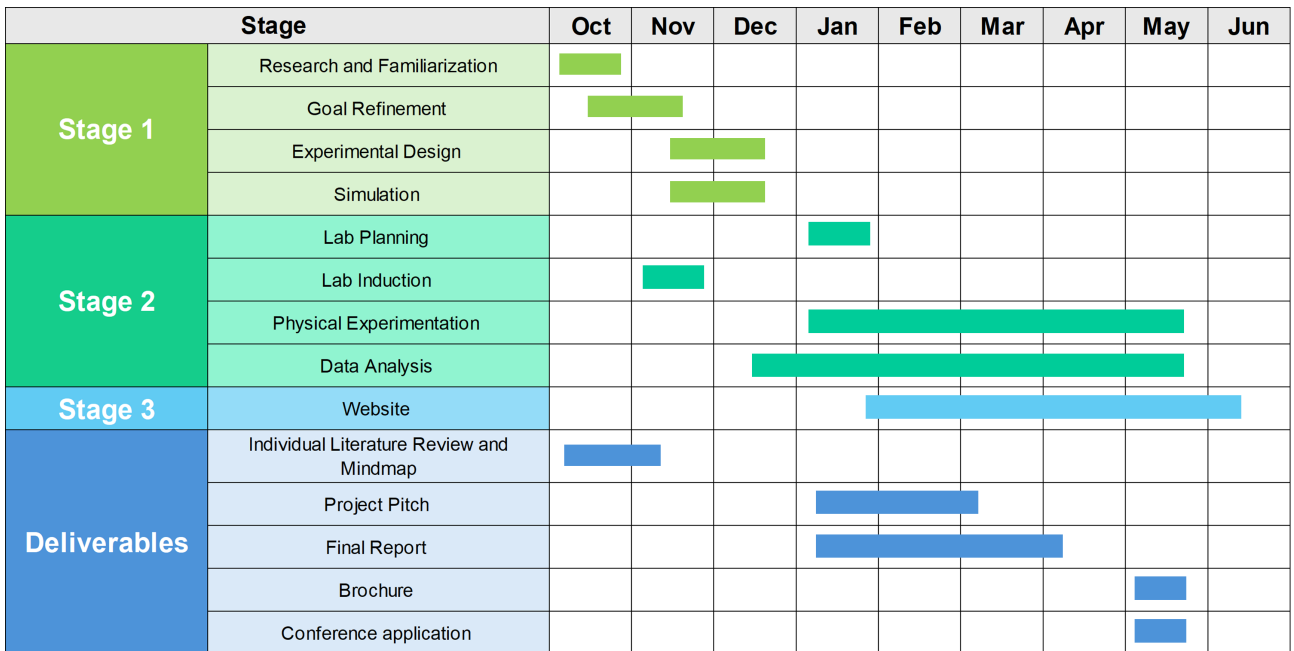


Figure 14: *Gantt Chart outlining the expected time frame of each section of the project.*

A. Appendix - Reflection

A.1. Project Management

The Gantt chart demonstrated by Figure 14 was instrumental in keeping the project on track to meet its objectives.

Despite initial enthusiasm, the team encountered several obstacles that hindered expected progress. Stage 1, Goal Setting, took longer than expected as a result of difficulties with defining the objectives and direction of the project.

After the project's direction had been clarified, the team quickly moved into Stage 2: Experimental Verification. However, issues emerged during this phase when the results from the initial system analysis did not align with the predictions made during the *in silico* simulations, as discussed in subsubsection 4.3.1. The group believes, as outlined in Section 5, that these discrepancies were likely due to errors during the simulation phase. To address this, three new G_i strands were selected and ordered. Unfortunately, there was a delay in the delivery of these strands. During this period, the team focused on completing the analysis of the original strands and initiated side projects, including website development.

Once the new strands arrived, the team was able to quickly run the new experiments and made significant strides in getting the project back on track before the submission of this report.

A.2. Key Project Management Lessons

- Firstly, one of the most valuable project management lessons we learned was the importance of establishing clear and effective communication channels. These channels proved crucial in allowing our team to resolve challenges quickly and maintain consistent progress. Several issues arose throughout the project, leading the team to develop a structured approach to problem solving. We would first attempt to resolve the issue

internally, either through discussion in our biweekly meetings or via our WhatsApp group chat. These informal channels allowed for rapid back-and-forth communication, enabling us to share suggestions in real time. If this was not sufficient, the issue was then escalated to our supervisors either in person or online, via our Microsoft Teams channel. As a result of this open communication strategy, our supervisors were more able to provide assistance, helping to ensure no issue went unresolved for too long.

2. Another key lesson learnt was the importance of effective time management in keeping a large, multi-faceted group project on track. Early in the project, we struggled to balance progress with our research with the high volume of both group and individual assignments. To help with this, a significant part of our internal meetings was dedicated to planning the work for the week ahead. When tasks were allocated, the group took time to ensure everyone fully understood their responsibilities and deadlines. This helped to ensure progress remained consistent, even when individual schedule became demanding. Alongside this, we deliberately set internal deadlines weeks in advance of the actual submission. This gave us a buffer to accommodate unexpected issues, and allowed us to receive and implement feedback from our supervisors. In turn, this led to a higher quality of work being submitted, improved productivity, and reduced stress of group members.
3. Finally, we learnt that by aligning individual goals with the broader objectives of the project, team members were more motivated and enthused by their work, leading to improved productivity. From the outset, all group members expressed an interest in developing their wet lab skills. With this in mind, tasks in the lab were rotated so everyone had the opportunity to develop these skills. Outside of the lab, it was decided that tasks would be assigned based on each member's unique strengths and expertise. By doing this, we were able to increase overall efficiency and also ensured everyone felt personally invested in their contributions. However, role allocations were always flexible, allowing team members to hop on and off sub-projects when help was needed or when they wanted to learn a new skill. This ensured engagement in the project was always strong, helping to produce consistently high-standards of work across the team.

B. Appendix - Calculation of Theoretical Rate Constants from ΔG

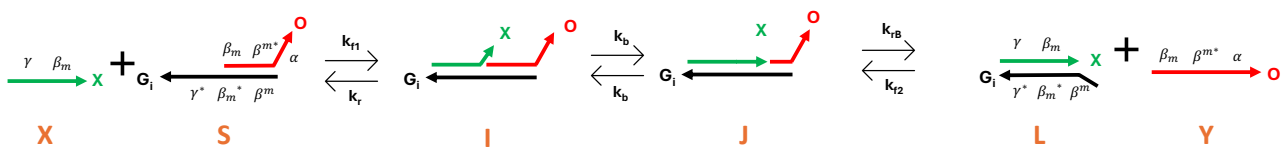


Figure 15: *Expanded Model Reaction System*. As illustrated, our primary reaction can be expanded to display the intermediate steps that occur throughout the toehold exchange process (denoted as complexes I & J). Each strand in this expanded system has been labelled with its identifier as in previous sections (namely X, O, and G_i). All toehold regions which have the potential to be hybridized (i.e. bound to a complementary region) are labelled along each strand with a corresponding domain name; complements are indicated with a *. In the reaction system, the invader strand X reacts with the substrate complex S and displaces the O strand (Y complex) by branch migration, resulting in the formation of complex L. The intermediates I and J are defined such that the reaction is considered to be in state I when strand Y is bound to more bases of the β_m toehold region than strand X. Complex J is defined as the inverse: more strands of β_m are bound to strand X than strand Y. As discussed in [Appendix B](#), for our system the m in β_m represent the incumbent toehold length and is equal to 2.

In [Figure 5](#), the bimolecular rate constant of a reaction is plotted against the associated Gibbs Free Energy (ΔG). To obtain the rate constant as a function of the ΔG , we rely on the model designed by Zhang et.al [25]. To do this, our reaction system can be represented as seen in [Figure 15](#) and expressed as the chemical reaction in [Equation B.1](#):



As part of the model, k_{f1} and k_{f2} are assumed to be equal in value; note that this assumption could be a source

of error in the outputs. For our purposes, we have taken $k_{f1} = k_{f2} = 3.5 \times 10^6$ based on fitted experimental data from Zhang et.al [25].

The rate constant k_b is the branch migration rate constant and can be calculated using [Equation B.2](#):

$$k_b = \frac{b}{(b-m)^2}. \quad (\text{B.2})$$

Where b is the total branch migration length and m is the incumbent toehold length. In our case, $b = 15$ and $m = 2$; hence $k_b = 1.3314$. In the model, k_{rB} is the first-order rate at which the toehold of the X strand dissociates, and is calculated using [Equation B.3](#):

$$k_{rB} = k_{f1} \cdot \frac{2}{(b-m)} \cdot e^{\Delta G^\circ(\beta^2)/RT} \quad (\text{B.3})$$

$\Delta G^\circ(\beta^2)$ refers to the binding energy between β^2 and its complement and was taken to be -2.7 based on values provided by Zhang et.al [25] for reactions where $m = 2$.

Conveniently, k_r can be calculated similarly, using an amended version of [Equation B.3](#) in which $\Delta G^\circ(\beta^2)$ is replaced by ΔG° , the free energy of the reaction for the G strand we are interested in ([Equation B.4](#)):

$$k_r = k_{f1} \cdot \frac{2}{(b-m)} \cdot e^{\frac{\Delta G^\circ}{RT}} \quad (\text{B.4})$$

The temperature of our reaction was set to 298K for modelling purposes, and the gas constant was taken as $1.987 \times 10^{-3} \text{ kcal}/(\text{mol} \cdot \text{K})$.



Using the model proposed by Zhang et.al [25] we could then calculate the forward rate constant for the simplified bimolecular version of our reaction system, denoted as $k_{forward}$ in [Equation B.5](#), by employing [Equation B.6](#):

$$k_{forward} = \frac{(k_{rB} \cdot k_f \cdot k_b)}{(k_r \cdot k_{rB} + k_r \cdot k_b + k_{rB} \cdot k_b)} \quad (\text{B.6})$$

Using this equation and the calculations for the intermediate step rate constants, we could then determine the forward rate constant for any given G_i strand design from its determined ΔG value.

C. Appendix - PMF Calculations

For the statistical analysis of ΔG mismatches presented in [Figure 6](#), the probability mass function of the free energies of strands with each number of mismatches was determined. This was done in MATLAB by applying the following steps:

1. Datasets of the ΔG values for strands with 1, 2, and 3 mismatches were collected, filtered for redundant strand sequences, and taken as an input to a new MATLAB file.
2. For each dataset, the ΔG values were plotted in a normalized histogram with a bin size of 0.2 kcal/mol.
3. The values of the mean ΔG and standard deviation from the mean were calculated using the appropriate MATLAB functions and plotted as vertical lines.

D. Appendix - Experimental Calibration & Preliminary Characterisation Reactions

D.1. Fluorescent Calibration - Linking Fluorescence and Experimental Concentrations

To generate fluorescent calibration curves, FQ and FO were loaded into a 96-well microplate. FQ was prepared at a range of final concentrations (0, 2, 4, 8, 10, and 20 nM). Fluorescence measurements were plotted to generate standard calibration curves using linear regression. The regression analysis and resultant slope and offset can be found in [Figure 16](#). Promisingly, the results of the fluorescent calibration confirms that the concentrations chosen (2-10 nM) are within the linear fluorescence region; a necessary outcome for simple conversion between fluorescence and concentration. These fitted parameters serve as the reference by which to convert fluorescence data into concentrations for analysis of reaction kinetics in all reaction systems tested within this report. A full breakdown of the procedure used to calibrate the system can be found in [P9.2](#).

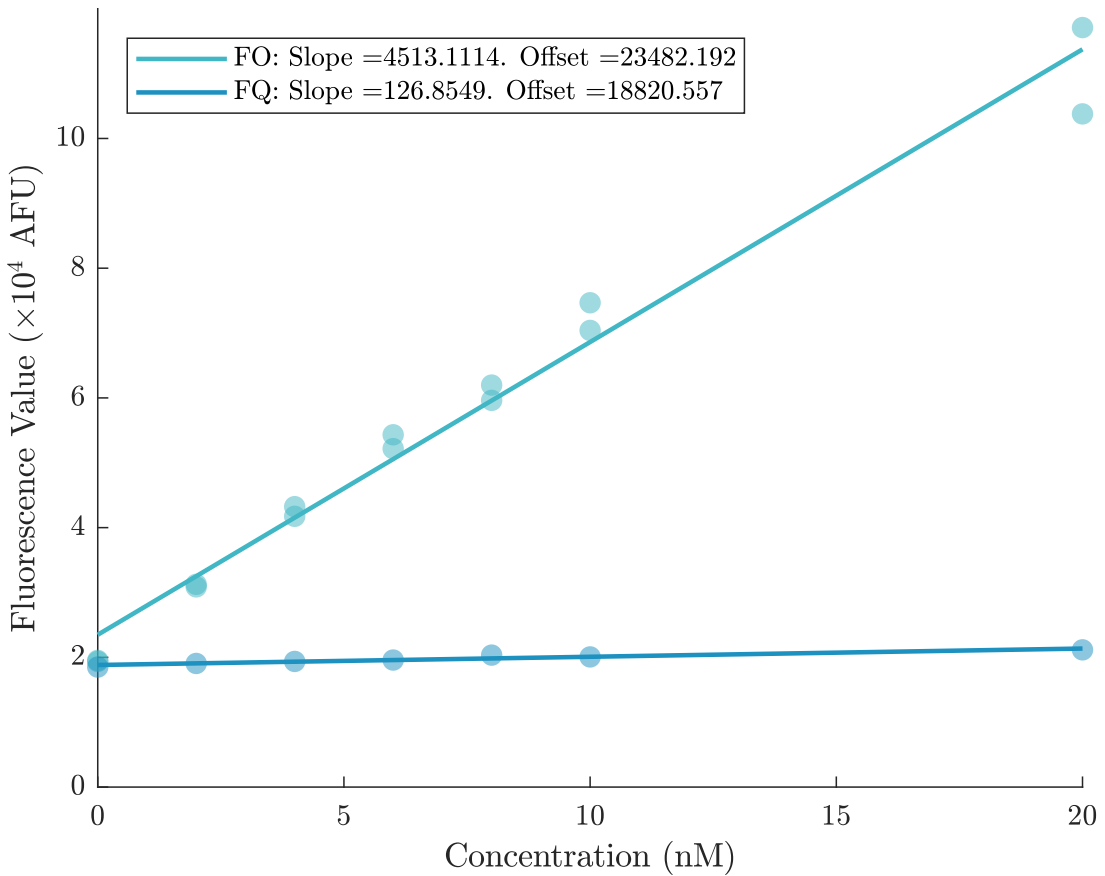


Figure 16: Fluorescence Values as a function of FO and FQ concentration during fluorescent calibration (as outlined in [P9.2](#)).

D.2. Reporter Complex Kinetic Characterisation

To determine the kinetics of the reporter reaction and verify that the kinetic profile is fast enough to capture the kinetics of the preliminary reaction system, different concentrations of the O strand were injected into microplate wells prepared with the FQ complex. Reaction progress was monitored, and the resulting data processed using the previously generated calibration curves. A breakdown of the full procedure used can be found in [P9.3](#).

When analysing the reporter characterisation, we observed that it was difficult to accurately fit the ODE model of our system ([Equation F4.1](#)) as the majority of the kinetic region was missed by the plate reader

measurements; i.e. the concentration of FO reached its maximum within one cycle of 26 seconds. If we required a precise estimate of the rate constant of the reporter system, we could adapt the experimental procedure to gather more data within the kinetic region. Both single-well readings with the POLARstar plate reader and stopped-flow measurements provide strong options to do this. However, for this experiment, we simply assume that the high speed of the reaction indicates a reporter system that will not limit our ability to record the kinetics of the main system.

D.3. Leak Reaction Testing

To confirm that no leak reaction occurs between the invader strand and the reporter complex, different concentrations of X were injected into microplate wells prepared with the FQ complex. The full procedure used to test for a leak reaction is found in P9.4. In comparison to the negative controls, no significant increase in fluorescence was observed, as evidenced by Figure 17. We therefore conclude that the invader strand does not react substantially with the reporter, and all fluorescence observed in the main system testing can be attributed to O strand interactions with the reporter complex.

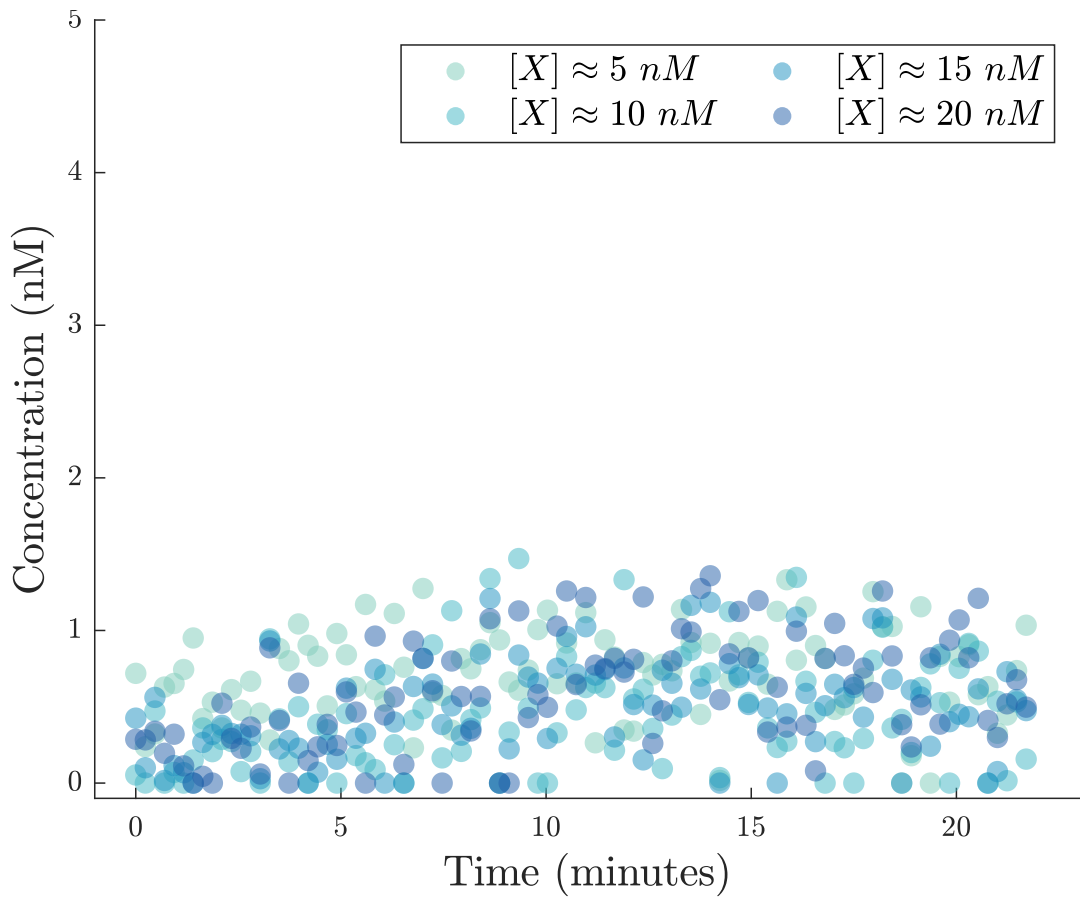


Figure 17: Experimental concentration of FO as a function of time during Leak Reaction Testing (as outlined in P9.4). $[X]$, as defined in the legend, is indicative of the concentration of G_iO present in each experimental sample. Concentrations presented represent average values taken from triplicate measurements for each experimental concentration of G_iO .

E. Appendix - Website design details

E.1. System Overview

The tool is implemented using a modular full-stack architecture, divided into a JavaScript-based frontend and a Python/Django-based backend.

E.2. CSV-based Sequence-Rate Database

A .CSV file serves as the core data storage system for this tool. It contains a curated library of DNA toehold sequences alongside their associated strand displacement rate constants (k), forming the basis for the prediction and matching engine shown in (Figure 18).

Sequence	Mismatch Count	DeltaG (kJ)	Rate (k)
ATTTAGGCGC	1	-13.035181	3380445.66
TTTTAGGCGC	1	-9.628370	2276876.90
CTTTAGGCGC	1	-8.016625	2975816.90
GTTTAGGCGC	1	-8.677198	3335153.79
AATTAGGCGC	2	-9.430068	3028310.00
ATTTAGGCGC	2	-13.035181	3470362.18
ACTTAGGCGC	2	-8.750070	3225658.67

Figure 18: .CSV file layout

The dataset was generated through simulations performed using the NUPACK software suite, as described in subsection 3.2. Each entry in the CSV includes a toehold sequence, its predicted rate constant, and relevant metadata such as the thermodynamic parameters.

This database forms a foundational component of the tool's functionality. By mapping sequence features to simulated rate constants, it enables the system to identify candidate toehold strands that closely match a user-defined kinetic target. The structured format also allows for efficient querying and filtering, supporting both exact matches and approximate solutions through interpolation.

The CSV format was chosen for its simplicity, transparency, and compatibility with both manual curation and programmatic access within the Django backend [51]. However, this may be replaced in future with a more robust and professional database solution such as MySQL or MongoDB, depending on scalability and performance requirements.

E.3. Python-Based Codebase

The core predictive engine of the tool is implemented in Python, managing the logic required to process user input, retrieve appropriate sequence data, and return a suitable toehold strand. This functionality is driven by

a script designed to identify the closest match to a user-specified rate constant using a lightweight, heuristic approach [51].

The core predictive engine of the tool is implemented in Python and is responsible for interpreting user input, accessing the sequence dataset, and returning a toehold strand that best matches the desired kinetic behaviour. This engine relies on a simple yet effective heuristic algorithm to select an appropriate candidate based on a user-specified strand displacement rate constant.

When a user submits a target rate constant (k), the backend loads the precomputed dataset from a .CSV file using the pandas library. Each row in the dataset corresponds to a toehold sequence and its associated properties, including energy, category, and predicted rate constant.

The algorithm calculates the absolute difference between the input rate constant and each entry in the dataset, selecting the toehold with the minimal difference. This process ensures that a kinetically appropriate candidate is returned quickly and with minimal computational overhead. The implementation utilises vectorised operations in pandas for efficiency.

This line subtracts the user-defined rate from each value in the “Rate Constant” column, takes the absolute value of the differences, and identifies the index of the minimum value. The corresponding row is then selected as the best match, and the associated toehold sequence is returned.

Following the identification of a matching sequence, the strand can be passed through a secondary structure validation step. This ensures that the selected toehold does not exhibit unwanted structural features such as hairpins, self-complementarity, or undesired intramolecular binding.

E.4. Django Framework

The Django web framework is used to structure the backend logic. It manages URL routing, API endpoint handling, and connections between the database, and user queries. Django was selected for its robust architecture, ease of scalability, and built-in support for REST APIs [52].

E.5. Django REST API

The Django REST API serves as the communication layer between the frontend and backend components of the tool. A REST API (Representational State Transfer Application Programming Interface) is a widely used web architecture that enables different parts of an application to communicate over HTTP using standard methods such as GET, POST, PUT, and DELETE [53]. In this context, the REST API allows the frontend interface to interact with backend logic and data processing in a structured and efficient manner. Additionally it allows for calling of external APIs such as NUPACK.

When a user enters a desired strand displacement rate constant through the web interface, the input is sent to the API as a JSON-formatted POST request. The API first validates the input to ensure it is a numerical value within an acceptable range, then passes it to the backend processing module.

The backend identifies the toehold sequence with the closest matching rate constant, it then performs a secondary structure analysis using the NUPACK software.

E.6. Frontend Architecture

The frontend of the tool will be a dynamic web interface developed using JavaScript. It is responsible for capturing user input, sending data to the backend via API calls, and displaying the output in a structured and accessible format.

Users are prompted to enter a desired rate constant, which may be extended in future versions to include additional parameters such as toehold length, GC content, or environmental conditions. Upon submission, the

frontend sends the input to the Django REST API using asynchronous HTTP requests, enabling a smooth, real-time user experience without the need to reload the page.

Once a response is received, the frontend renders the output clearly and interactively. This includes: The predicted toehold DNA sequence, a visual representation of the designed strand, a pass/fail indicator showing whether the sequence exhibits secondary structures, this is visualised in [Figure 13b](#).

This design ensures fast feedback and ease of use for a range of users, from researchers to students in synthetic biology.

E.7. Design Considerations

The development of the tool was guided by several key design principles aimed at ensuring functionality, reliability, and ease of use. Modularity was a core consideration, with the system structured such that the frontend, backend, database, and prediction engine function as independent components. This separation allows for easier testing, maintenance, and future upgrades.

In terms of usability, the interface will be designed to accommodate a broad range of users, including those without a programming background. The input process will be kept minimal and intuitive, making the tool suitable for both educational and research settings. To validate this, we will conduct user acceptance tests to ensure that the interface meets the needs and expectations of its intended audience.

Finally, transparency and interpretability were essential design goals. The prediction logic is deliberately simple and clearly documented (see supplemental information section), allowing users to understand and trace how output sequences are selected, an important aspect in both experimental planning and result validation.

E.8. Deployment Strategy

To ensure that the application scales to a large number of users while remaining easy to maintain, we intend to deploy the tool using cloud infrastructure provided by Amazon Web Services (AWS). AWS serves as both the server host and cloud provider, enabling the application to be accessed globally via the internet.

The deployment is centred around Amazon EC2 (Elastic Compute Cloud), which provides a configurable virtual server environment. The EC2 instance will host the Django backend, serve the REST API, and deliver the static frontend files. This approach allows full control over the runtime environment, including system dependencies and application-level configurations [54].

To enable global accessibility, the tool will be hosted online and accessible from any location with an internet connection. This supports collaboration across institutions and research environments. As part of this deployment, a dedicated domain will be required to provide users with a consistent and secure access point. Scalability is built into the system through the use of Amazon EC2, which enables the server instance to be resized or upgraded to accommodate increased processing demands or higher user traffic.

Additionally, the solution provides a high degree of customisability and control. The virtual server environment can be tailored to meet the specific technical requirements of the application, including software dependencies, package configurations, and system performance tuning. Finally, maintenance and reliability are enhanced through AWS infrastructure services, which offer monitoring tools, uptime management, and automated recovery options, all of which contribute to the robustness and stability of the deployed tool.

Deploying via AWS also removes reliance on local hardware or university-hosted services (such as CSU), offering a more scalable and flexible alternative for production-ready deployment.

Standard Experimental Procedure for the Determination of Rate Constants of Strand Displacement Reactions

BIOREGEN Experimental Protocol - 2025

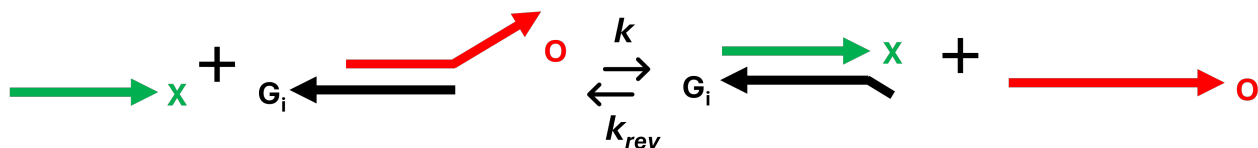
P6. Introduction

This document is intended to be used as the standard procedure for the experimental testing of the DNA toehold exchange reaction system designed by the BIOREGEN Project Group. The document can also serve as a reference for others wishing to conduct research into toehold exchange reaction systems.

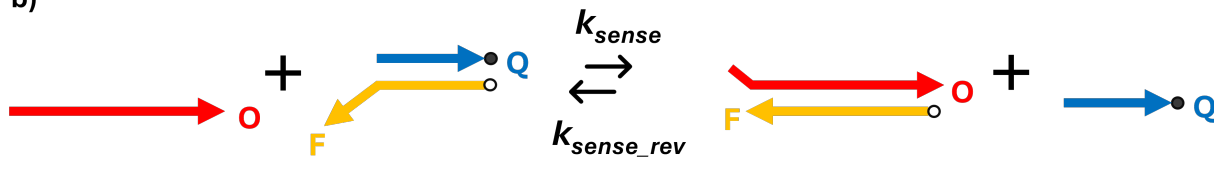
By applying the following procedure, the project group aims to experimentally build a library of toehold exchange strands and capture their reaction rates over several orders of magnitude. To achieve this, the measure of fluorescence from an ATTO 565 fluorophore will be used to track reaction progression. Data from the fluorescent reaction tracking will be used to extract rate constants from fitted data to experimentally verify theoretical simulation done in NUPACK.

A diagram of the full reaction system is demonstrated by Figure 19.

a)



b)



- Quencher
- ATTO 565 Fluorophore

Figure 19: The full BIOREGEN reaction system for tuning and measuring kinetic rate constants of strand displacement reactions. The design consists of two toehold exchange reactions which are set up together and run simultaneously. For the secondary reaction to occur, the preliminary reaction must first execute successfully (a) The primary reaction of interest. In this reaction, the displacement of the O strand is facilitated by the invader, X. The letter k represents the rate constant to be fitted and measured for the system. (b) The reporter system in which the displaced incumbent strand O from the primary reaction reacts with reporter complex FQ. The result of this secondary reaction is a fluorescent signal produced by unquenched fluorophore molecules that is proportionate to the concentration of the first system that has successfully reacted.

P7. Experimental Summary

Note: The experimental procedure section of this document can be used as the method for all reactions/experiments conducted by the BIOREGEN team. Stages 1 (Preparation) and 2 (Annealing) are the same for every experiment, while Stage 3 (Plate Reader Setup & Use) differs slightly for each experiment conducted. For details about specific plate reader configurations please refer to the experiment-specific instructions in P9.

General Overview:

1. Create standard curves for relevant fluorescent species
2. Prepare initial solutions
3. Prepare all complexes and allow thermal equilibrium to be reached
4. Set up the experimental well plate with all initial complexes
5. Introduce injector species to trigger the reaction
6. Oversaturate the system - Nuking
7. Analyse data and extract appropriate rate constants

Step	Purpose	Reactant (Volume, Expected Concentration in 200 μL) (nM)	Total Volume (μL)
Initialisation	Initial Step: Reactant + Buffer	First Reactant: 150 μL , 10 nM	150
Reaction Trigger	Adding Invader	Invader Species: 50 μL , 2-10 nM	200
Oversaturation (Nuking)	Oversaturating Concentration of Invader	Invader species: 10-20 μL , 50 nM	210-220

Table 7: *Summary of the primary reaction steps, expected reactant volumes, and full system volumes for each stage of the reaction.*

Note: The nuking step noted in Table 7 can be defined as the process by which the original system is saturated with invader strand molecules. The main aim of this step is to drive the thermodynamic equilibrium towards the product species and ensure most of the original concentration of gate strands will successfully react. This is also a way to verify that the system works as desired since direct comparison with the positive controls allows this final step to verify whether the original concentrations of gate strand were as intended or not.

P8. Experimental Procedure: All Characterisations

P8.1. Stage 1: Preparation

An overview of steps taken to create the necessary solutions and prepare the well plate for reaction.

Task: Prepare sample solutions from DNA strand stocks using the Dilution Equation (Equation P8.1).

Note: Buffer formulation steps can be found in P10.1.

$$M_1 \cdot V_1 = M_2 \cdot V_2 \quad (\text{P8.1})$$

Sample Preparation Procedure:

1. Maintain a clean, contaminant-free workspace to ensure the integrity of the experiment.
2. Prepare a 1 mL, 2 μM dilution for each DNA strand stock ordered from IDT.

Note: Do this for each relevant DNA strand used in the reaction being conducted. Which strands to prepare can be found in the reaction specific part of the document ([P9](#)).

3. Dilutions should be brought to the desired 1 mL volume using prepared TAE buffer solution or nuclease-free TE buffer at pH = 7.5 to ensure better stability of the dilution.

Note: Salts (1 M NaCl) are added to buffers that are used for double stranded DNA to stabilise the complexes, single stranded DNA is buffered in pure TAE. The total stock volume required to do this can be calculated using [Equation P8.1](#) or by referencing [Table 8](#) for all strands used in BIOREGEN-specific reactions.

Strand	Stock	Final Concentration	Total Volume	Stock Volume Needed
X	100 uM	2 uM	1 mL	200 μL
O	100 uM	2 uM	1 mL	200 μL
Q	100 uM	2 uM	1 mL	200 μL
F	100 uM	2 uM	1 mL	200 μL
G_{init}	100 uM	2 uM	1 mL	200 μL
G_{1e1}	100 uM	2 uM	1 mL	200 μL
G_{1e2}	100 uM	2 uM	1 mL	200 μL
G_{1e3}	100 uM	2 uM	1 mL	200 μL
G_{1e4}	100 uM	2 uM	1 mL	200 μL
G_{1e5}	100 uM	2 uM	1 mL	200 μL
G_{1e6}	100 uM	2 uM	1 mL	200 μL
G_{1e3*}	100 uM	2 uM	1 mL	200 μL
G_{1e2*}	100 uM	2 uM	1 mL	200 μL
G_{4e1*}	100 uM	2 uM	1 mL	200 μL

Table 8: Summary of the volumes required for the dilution of DNA strand stock dilutions for strands used within the BIOREGEN experimental verification.

P8.2. Stage 2: Annealing

NanoDrop Procedure:

Overview: Prior to annealing the strands, a NanoDrop spectrophotometer is used to calculate the true concentration of the dilutions prepared in [P8.1](#).

Task: Verify the true concentrations of the samples. Adjust sample concentration if there are significant deviations from the 2 μM intended concentration.

1. Set NanoDrop sample type to ‘ssDNA’ (single-stranded DNA).
2. Clean machine with pure water and use a plain buffer solution to calibrate by running a “blank”.
3. Check the absorbance of each prepared strand solution (at $\lambda = 260 \text{ nm}$) 3 times per sample (or however many required for the results to be reasonably stable), and calculate the average absorbance.

4. Use the average absorbance to calculate concentrations for each diluted solution using the Beer-Lambert Law ([Equation P8.2](#)).

- For all calculations:

a) Take the optical path length (l) to be 1 cm.

b) Obtain the appropriate molar absorption coefficient from the strand data sheet for each calculation. For ease, molar absorption coefficients of the BIOREGEN system can be found in [Table 9](#).

5. After computing the concentration, compare the calculated concentration with $2 \mu\text{M}$. If the solution is significantly more concentrated, dilute again using TAE buffer to obtain a concentration close to $2 \mu\text{M}$ and perform steps 1-5 for the new dilution.

$$A = \varepsilon \cdot c \cdot l \quad (\text{P8.2})$$

where:

A is the Absorbance

ε is the Molar absorption coefficient ($M^{-1}cm^{-1}$)

c is the Molar concentration (M)

l is the Optical path length(cm)

Strand	Molar Absorption Coefficient ($\varepsilon - L / (\text{mole}\cdot\text{cm})$)
O	252,600
X	207,800
F	281,300
Q	160,100
G_{init}	251,300
G_{ke1}	251,500
G_{ke2}	254,500
G_{ke3}	253,300
G_{ke4}	253,100
G_{ke5}	252,900
G_{ke6}	261,800
G_{1e3^*}	252,600
G_{1e2^*}	255,300
G_{4e1^*}	255,300

Table 9: *Molar Absorption Coefficient Values of DNA strands in the BIOREGEN reaction systems. G_{1e3^*} , G_{1e2^*} , G_{4e1^*} indicate the new, redesigned strands. The rest of the G_i strand molar absorption coefficient values correspond to the initial G_i strands in the first round of the experiment.*

Thermocycler Procedure:

Overview: Taking the strand solutions prepared in Stage 1, a ThermoFisher ProFlex thermocycler is used to denature and anneal the appropriate strands in preparation for the reaction we wish to study.

Task: Use the thermocycler to assemble the required DNA complexes.

1. Place prepared samples into an unoccupied block in the thermocycler.

2. Select the relevant cycling procedure.

- For the BIOREGEN system, the relevant cycling procedure involves samples being raised to a temperature of 95°C and then gradually cooled to 4°C over a period of 80 minutes.

3. Close and label the relevant block. Start the block cycle.
4. Once completed, remove samples and use immediately or refrigerate/freeze for future use.

Note: In the BIOREGEN system, the invader strands (X) remain single stranded and do not need to be processed in this step. The G_i and O strands are denatured and annealed (with the O strand kept in 20% excess to ensure all G_i strands will be annealed) to form G_iO – this will be done separately for each G_i strand being tested. The O and F strands are denatured and annealed (with the O strand kept in 20% excess to ensure all F strands are annealed) to form the FO complex. The F and Q strands are denatured and annealed (with the Q strand kept in 20% excess to ensure all F strands will be annealed) for the formation of the FQ complex.

P8.3. Stage 3: Plate Reader Setup & Use

Overview: Outline of steps required to set up the well plate with the appropriate reactants and prepare the plate reader for injection of invader strand and subsequent measurement.

1. Preparation: Add 150 μL of initial reactant solution as outlined in the corresponding initial setup table in the relevant reaction specific section later in this document ([P9](#)).
2. Reaction triggering step: Add an additional 50 μL invader solution to each relevant reaction well to bring the total concentration of invader to the appropriate level. The desired concentrations are outlined in the relevant reaction-specific procedure ([P9](#)). This is done by injecting appropriately proportioned volumes of invader strand (at 200 nM) and buffer into each well. For positive and negative controls, 50 μL of buffer solution is injected in place of the invader strand. All wells should have a final volume of 200 μL .

Note: This injection step is completed by the POLARstar.

3. Nuking Step 1: Add an additional 10 μL of invader strand to all relevant reaction wells. Ensure that the concentration of invader strand solution being injected is greater than or equal to 200 nM. For all positive and negative control wells, add 10 μL of buffer solution. The final volume of each well should then be 210 μL .

Note: All nuking stages have to be completed by hand.

4. Nuking Step 2 (Optional): If testing a reaction system with two reaction steps (i.e. the primary reaction system as outlined in [P9](#)) you then need to perform a second nuking step of the secondary reaction. Add an additional 10 μL of the secondary invader strand (for the BIOREGEN system, this is the O strand which interacts with the FQ reporter complex). Ensure that the concentration of solution being injected is greater than or equal to 200 nM. The final volume of each well should then be 220 μL .

Note: The desired concentrations/volumes to be added to each well, including the invader/nuking agent, are outlined in their respective subsection in [P9](#) below.

[Figure 20](#) demonstrates the results you should obtain from running a reaction system with a single nuking step in the POLARstar plate reader [[55](#)].

Well Plate Setup

Task: Fill well-plate with required solutions for reaction initiation.

1. Dispense initial reactants (depending on reaction being performed) into separate reaction wells as outlined in the corresponding tables in [P9](#).

Note: Ensure wells are free of dust and pre-equilibrated to desired temperature prior to adding any reactants.

2. Cover the well plate with a microplate seal, making sure to align the seal with the plate and press firmly

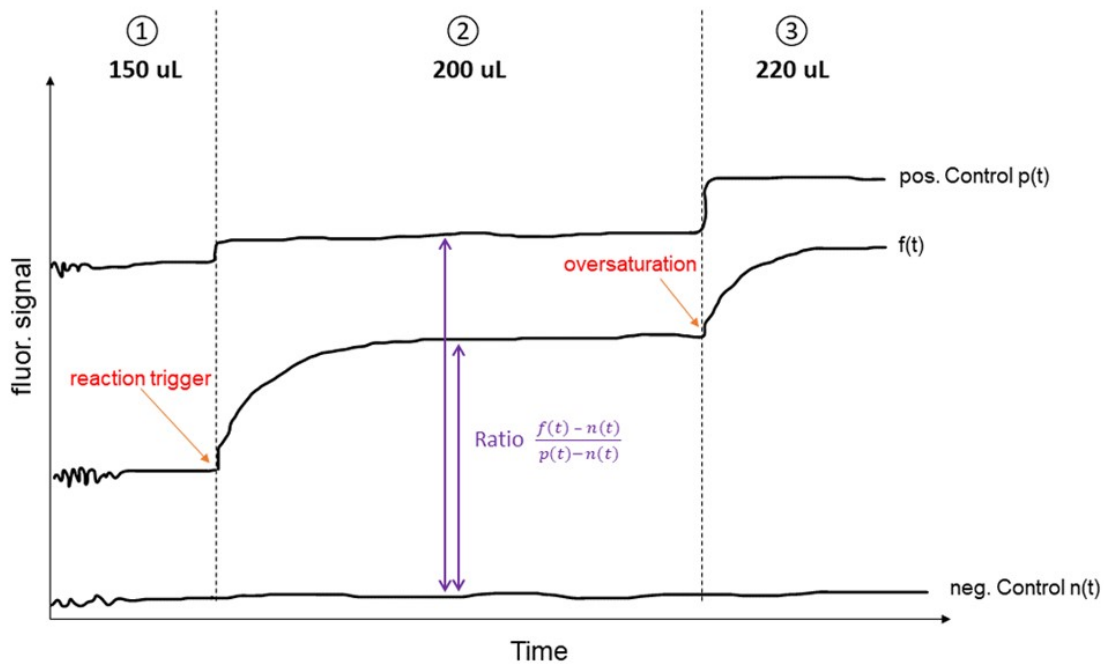


Figure 20: *Expected fluorescent signal output for a general DNA strand displacement reaction. The depiction includes three reaction stages: preparation and initial measurement; reaction initiation and progression; and a singular nuking stage. Well plate volumes are indicated at the top of each phase and the reaction trigger and oversaturation points are labelled in red. Three traces are depicted in the visual, namely the positive control, negative control, and experimental reaction. The representation resembles the expected output for the BIOREGEN reaction system. Reprinted from Standard Experimental Procedure for Strand Displacement Reactions, by K. Jurinović 2024 [55].*

to ensure a seal. This prevents evaporation of solvent from impacting the measured concentrations.

Note: Do not cover with a seal if something is being injected into the plate. In this case the lid of the well plate may be left on between injection rounds for longer reactions to prevent major evaporation.

3. Place the well plate into the plate reader, aligning the top left corner of the well plate with the frame of the plate reader.

POLARstar Setup

Task: Clean and set-up POLARstar plate reader for use

1. Cleaning: Before priming each injector, needles and tubing must be cleaned as follows:

- Using the “Prime” function or the internal buttons (labelled 1 and 2) execute a pump action and flush ethanol through the full tubing of each injector 3 times.
- Flush the ethanol out of the tubing by executing 3 pump actions to remove all fluid from the tubing.
- Ensure all generated waste is disposed of in an appropriate receptacle.
- Additional Steps for Specific Injector Fluid:
 - For injectors being used with buffer:

- a) Execute 3 pumping actions to flush 1xTAE 1M NaCl buffer solution through the tubing and into a waste receptacle.
- b) The needle is now primed with buffer solution and can be inserted into the appropriate hole in the base of the plate reader.
- For injectors being used with DNA:
 - a) Execute 3 pumping actions to flush 2% Bovine Serum Albumin (BSA) buffer solution through the syringe and tubing. Note that BSA solution must be kept in the fridge when not in use to prevent degradation.
 - b) Wait 15 minutes to allow solution to fully coat tubing.
 - c) Flush the BSA buffer solution out of the tubing by executing an additional 3 pump actions to remove all fluid from the tubing.

Note: This step is crucial to ensure that DNA strands will not stick to the internal lining of the syringe and tubing. However, BSA forms bubbles and it is therefore crucial that it is flushed from the injectors after successful coating of the injector.

- Execute 3 pumping actions to flush 1 x TAE, 1 M NaCl buffer solution through the tubing and into a waste receptacle.
- Pump 3 more times to remove the buffer from the needles.
- If injecting (as specified in the reaction-specific section – P9), prime the injector using 200 nM of injector species - make sure to inject the injector species back into the tube (forming a loop) so that no DNA strand solution is wasted. Execute pump action at least 3 times to ensure there are no bubbles and the plate reader is ready to inject.

2. POLARstar Reaction Preparation

- Preparing the plate reader:
Go to Manage Protocols → Test1 → Edit.
In each tab, ensure parameters match the following (Ignore any input boxes not mentioned here):
 - a) Basic Parameters: Should remain the same for each experiment.
In the *Protocol Name*, state Test1. For *Microplate boxes*, select BMG LABTECH 96.
In the *Filter settings* section, make *No. of multichromatics* equal to 1. Set the *Excitation filter* and *Emission filter* boxes to 550-10 and 590-10 respectively.
In the *Well Scan* box, select *Orbital average* and set the *diameter* to 4 mm.
In the *Optic* section, select *Bottom optic*.
In *General Settings*, set *Setting time* to 0.5 and *No. of kinetic windows* to 1.
In *Kinetic Window 1*, set *No. of cycles* to 999, *Measurement start time* to 0.0, *No. of flashes* to 17 and *Cycle time* to 92.
 - b) Layout: set the well plate diagram according to your well plate.
In the panel on the left, for *Content*, select Sample.
In the *Index* box, set the *start value* to 1 and select *Increase*.
In the *Replicates* box, set the *number* to 1 and select *Horizontal*.
 - c) Concentrations and volumes: This is where you input what volumes of the injecting solution you want. Volume 1 typically corresponds to the invader strand, and volume 2 represents the buffer. Ensure these values are correct for the experiment you are running, referring to P9.
 - d) Injection timing: Can set as you see fit. Ensure the positive controls have hit a steady-state value before anything injects, typically after around 15 minutes (20-40 cycles). Check that the box marked *Equidistant kinetic cycles* is selected.
 - e) Shaking: Set shaking to occur before the first cycle. Check *shake mode* is set to double orbital

and *frequency* is 300 rpm.

- f) Return to the *Basic Parameters* tab, press “check timing” in the bottom left-hand corner. Make sure the value matches the value listed in the *Cycle time* box in the *kinetic window 1* section.
 - g) You are now ready to run the reaction. Click *start measurement* in the bottom right-hand corner, select OK. A pop-up box will appear asking for additional inputs. Set the gain by calibrating such that a known concentration will result in a certain percent saturation of the fluorescent signal, or use a pre-established gain. For the BIOREGEN system, the gain is set to 2788.
 - h) Click “Start Measurement” and let the reaction commence.
- Injection & Nuking
 - a) All injection will be completed automatically by the POLARstar if you set up the reaction as outlined in the POLARstar Reaction Preparation section above. Only once the reaction reaches a steady-state value post injecting will you be ready for the first round of nuking. All nuking is done by hand.
 - b) Press pause (not STOP). Eject the well plate. Pipette the nuking volumes according to the specifications outlined in the table in the respective reaction-specific method (**P9**). Return well plate and press “Continue Run” (the measurements will continue where you left off).
 - c) If the specific reaction requires a secondary nuking step, repeat Step (b) for the second nuking agent after the first nuking cycle has been completed and the reaction has once again reached a steady state.
 - d) Once the reaction and nuking process are complete; press pause, let the current cycle finish, then press stop. There will be an option to save the unfinished test run data – PRESS SAVE.
 - e) Close the monitoring window and open the data in the MARS software. Click “Open Most Recent Test Run” from the plate reader software or navigate to the appropriate file in the MARS file list.
 - f) Export the data. To do this, ensure that the raw data is selected, not an average. Select all data points and open in an .xls file. Save the generated spreadsheet accordingly.
 - g) Clean the plate reader injectors by washing out with NaCl/TAE buffer 3 times, then ethanol 3 times.

P9. Reaction Specific Methods

P9.1. Main Reaction Protocol

Overview: Add the invader strand X at varying concentrations to initiate strand displacement reactions. Monitor fluorescence signals in real time. This ‘Standard Reaction’ is comprehensive for the whole reaction system outlined in *Figure 19*.

The Main Reaction utilises all possible strand solutions. The invader strand X solution needs to be prepared at 200 nM and with a minimum volume of 1 mL to later be injected. The FQ, FO and G_iO complexes all need to be prepared and annealed. The incumbent strand O needs to be prepared for nuking. The buffer being used in this reaction is the combination TAE and NaCl buffer. **Table 10** summarises which steps these strands are used in for the main reaction.

The well plate set up should resemble **Table 11** before reaction. Note in this reaction there are two negative controls; one with the FQ reaction complex and buffer, and another with just buffer on its own. This was done to establish baseline fluorescence and ensure the FQ reaction did not exhibit significant fluorescence on its own.

Reaction Step	Involved Strands/Complexes
Annealing	FQ, FO & GiO complexes.
Injecting	X and Buffer
Nuking	X and O

Table 10: Overview of reaction steps and required strand sequences for analysis of the BIOREGEN reaction system as part of the Main Reaction System Protocol.

	1	2	3	4	5	6	7	8	9	10	11	12
A	NC 10 μL FQ 140 μL buffer	NC 10 μL GiO 10 μL FQ 130 μL buffer	X₁ 10 μL GiO 10 μL FQ 130 μL buffer	X₂ 10 μL GiO 10 μL FQ 130 μL buffer	X₃ 10 μL GiO 10 μL FQ 130 μL buffer	X₄ 10 μL GiO 10 μL FQ 130 μL buffer	X₅ 10 μL GiO 10 μL FQ 130 μL buffer	PC 5 μL FO 145 μL buffer	PC 10 μL FO 140 μL buffer	PC 15 μL FO 135 μL buffer	PC 20 μL FO 130 μL buffer	NC 150 μL buffer
B			X₁ 10 μL GiO 10 μL FQ 130 μL buffer	X₂ 10 μL GiO 10 μL FQ 130 μL buffer	X₃ 10 μL GiO 10 μL FQ 130 μL buffer	X₄ 10 μL GiO 10 μL FQ 130 μL buffer	X₅ 10 μL GiO 10 μL FQ 130 μL buffer	PC 5 μL FO 145 μL buffer	PC 10 μL FO 140 μL buffer	PC 15 μL FO 135 μL buffer	PC 20 μL FO 130 μL buffer	
C			X₁ 10 μL GiO 10 μL FQ 130 μL buffer	X₂ 10 μL GiO 10 μL FQ 130 μL buffer	X₃ 10 μL GiO 10 μL FQ 130 μL buffer	X₄ 10 μL GiO 10 μL FQ 130 μL buffer	X₅ 10 μL GiO 10 μL FQ 130 μL buffer	PC 5 μL FO 145 μL buffer	PC 10 μL FO 140 μL buffer	PC 15 μL FO 135 μL buffer	PC 20 μL FO 130 μL buffer	

Table 11: Pre-Experimental Well Plate Setup for Main BIOREGEN Reaction System testing. Purple represents the volume of FQ required. Green is for the volume of GiO needed. Orange indicates the volume of FO required. The buffer volume needed is indicated in blue.

Injecting and nuking stages should resemble Table 12 for the standard reaction, assuming all stock solutions used for the injection step are at a concentration of 200 nM.

Finish and save results from the reaction as outlined above.

P9.2. FQ Fluorescence Calibration

Overview: The general experimental steps required for the fluorescent calibration of the reporter system used in all BIOREGEN experimentation.

1. Anneal 200 μ L of FQ and FO at 200 nM concentration. Organise well plate as outlined in Table 14, with buffer solution of both TAE and NaCl (for instructions on how to make this buffer, see P10.1).
2. Test the FQ reaction complex in one row, and the FO reaction complex in two duplicate rows. Measure fluorescence intensity (in arbitrary fluorescence units – AFU) using the PolarStar plate reader.
3. The resulting data should be exported and plotted to generate standard curves of fluorescence versus concentration for both FQ and FO.
4. Use linear regression to determine the slope and offset. These standard curves serve as references for

	1	2	3	4	5	6	7	8	9	10	11	12
A	NC Inject: 50 μ L buffer Nuke1: 10 μ L buffer Nuke2: 10 μ L buffer	NC Inject: 50 μ L buffer Nuke1: 10 μ L buffer Nuke2: 10 μ L buffer	X₁ Inject: 2 μ L X1 48 μ L buffer Nuke1: 10 μ L X1 10 μ L O	X₂ Inject: 4 μ L X1 46 μ L buffer Nuke1: 10 μ L X1 10 μ L O	X₃ Inject: 6 μ L X1 44 μ L buffer Nuke1: 10 μ L X1 10 μ L O	X₄ Inject: 8 μ L X1 42 μ L buffer Nuke1: 10 μ L X1 10 μ L O	X₅ Inject: 10 μ L X1 40 μ L buffer Nuke1: 10 μ L X1 10 μ L O	PC Inject: 50 μ L buffer Nuke1: 10 μ L buffer Nuke2: 10 μ L buffer	NC Inject: 50 μ L buffer Nuke1: 10 μ L buffer Nuke2: 10 μ L buffer			
B			X₁ Inject: 2 μ L X1 48 μ L buffer Nuke1: 10 μ L X1 10 μ L O	X₂ Inject: 4 μ L X1 46 μ L buffer Nuke1: 10 μ L X1 10 μ L O	X₃ Inject: 6 μ L X1 44 μ L buffer Nuke1: 10 μ L X1 10 μ L O	X₄ Inject: 8 μ L X1 42 μ L buffer Nuke1: 10 μ L X1 10 μ L O	X₅ Inject: 10 μ L X1 40 μ L buffer Nuke1: 10 μ L X1 10 μ L O	PC Inject: 50 μ L buffer Nuke1: 10 μ L buffer Nuke2: 10 μ L buffer				
C			X₁ Inject: 2 μ L X1 48 μ L buffer Nuke1: 10 μ L X1 10 μ L O	X₂ Inject: 4 μ L X1 46 μ L buffer Nuke1: 10 μ L X1 10 μ L O	X₃ Inject: 6 μ L X1 44 μ L buffer Nuke1: 10 μ L X1 10 μ L O	X₄ Inject: 8 μ L X1 42 μ L buffer Nuke1: 10 μ L X1 10 μ L O	X₅ Inject: 10 μ L X1 40 μ L buffer Nuke1: 10 μ L X1 10 μ L O	PC Inject: 50 μ L buffer Nuke1: 10 μ L buffer Nuke2: 10 μ L buffer				

Table 12: *Injecting/Nuking protocols for Standard Reaction.* The volume of buffer required is in blue. Green represents the volume of the incumbent strand O. The volume of the invader strand X required is outlined in brown.

converting fluorescence signals into strand concentrations in subsequent kinetic analyses.

The strands used in this reaction include the FQ and FO reaction complexes. The buffer used here is the combination TAE and NaCl buffer. **Table 13** summarises at what stage the strands are used in the Fluorescence Calibration reaction.

Table 14 demonstrates the well plate setup for the Fluorescence Calibration reaction.

Reaction Step	Involved Strands/Complexes
Annealing	FQ & FO complexes
Injecting	None.
Nuking	None.

Table 13: *Outline of reaction steps and required sequences for the FQ Fluorescence Calibration reaction.*

P9.3. Reporter Complex Characterisation

Overview: The experimental steps for the reporter characterisation reaction.

- First, insert the plate into the plate reader to measure the baseline fluorescence signal before reaction initiation. **Table 16** outlines the initial well plate setup.

Note: Well 1 serves as the negative control, containing only 150 μ L of buffer solution (TAE + NaCl). This control is used to establish the baseline fluorescence signal in the absence of any background fluorescence.

	1	2	3	4	5	6	7
A	FQ 0 nM 0 μ L 150 μ L buffer	FQ 2 nM 2 μ L 148 μ L buffer	FQ 4 nM 4 μ L 146 μ L buffer	FQ 6 nM 6 μ L 144 μ L buffer	FQ 8 nM 8 μ L 142 μ L buffer	FQ 10 nM 10 μ L 140 μ L buffer	FQ 20 nM 20 μ L 130 μ L buffer
B	FO 0 nM 0 μ L 150 μ L buffer	FO 2 nM 2 μ L 148 μ L buffer	FO 4 nM 4 μ L 146 μ L buffer	FO 6 nM 6 μ L 144 μ L buffer	FO 8 nM 8 μ L 142 μ L buffer	FO 10 nM 10 μ L 140 μ L buffer	FO 20 nM 20 μ L 130 μ L buffer
C	FO 0 nM 0 μ L 150 μ L buffer	FO 2 nM 2 μ L 148 μ L buffer	FO 4 nM 4 μ L 146 μ L buffer	FO 6 nM 6 μ L 144 μ L buffer	FO 8 nM 8 μ L 142 μ L buffer	FO 10 nM 10 μ L 140 μ L buffer	FO 20 nM 20 μ L 130 μ L buffer

Table 14: Overview of the general well plate set up of all required volumes and concentrations used for the FQ Fluorescence Calibration. Purple represents the FQ complex volume and concentration. Blue is for the volume of buffer required. Green represents the volume and concentration needed of the FO complex.

Wells 8 to 11 serve as positive controls, each containing different concentrations of FO complex diluted in buffer solution to obtain a total volume of 150 μ L.

These wells provide reference points for maximum fluorescence output at known concentrations.

- Once steady-state values are reached, injection can begin. For wells 2 to 7, this injection consists of varying volumes of invader strand O diluted with buffer, such that the final volume in each well comes to 200 μ L. Wells 1 and 8–11 are injected with 50 μ L of pure buffer to keep the volume consistent. Table 17 outlines this process.
- Record fluorescence in real-time, process the resulting data using the previously established calibration curves and the data analysis method outlined in P10.1 to compute the reaction rate constant.

Both the FQ and FO complexes are required for this reaction. The incumbent strand O becomes the invader strand and displaces Q. The buffer used in this reaction is the combination TAE and NaCl buffer. Table 15 outlines which DNA solution is needed for which step in the Reporter Complex reaction.

Reaction Step	Involved Strands/Complexes
Annealing	FQ and FO complexes. Invader strand O.
Injecting	O and Buffer
Nuking	None.

Table 15: Outline of reaction steps and strand required for the Reporter Complex Reaction.

Table 16 and Table 17 outline the initial well plate setup and injecting requirements for the reporter complex characterisation.

P9.4. Leak Reaction

Overview: Assessing whether the Reporter Complex (FQ) and Gate Complex ($G_{init}O$) strands are reacting to cause a false fluorescence signal to be emitted. Specifically, we want to ensure that the O strand is not displacing the Q strand without first being triggered by the invader X. The unblocked fluorophore complex (FO) acts as a positive control.

Note that the G_i strand used in this experiment was G_{init} , the original gate strand with no toehold mismatches (i.e. perfect complementary).

For full procedural breakdown, see above sections. A quick overview is below.

- Prepare a 2 μ M dilution for each DNA strand from stock strands

	1	2	3	4	5	6	7	8	9	10	11
A	NC 150 μL buffer	10 μL FQ 140 μL buffer	PC 5 μL FO 145 μL buffer	PC 10 μL FO 140 μL buffer	PC 15 μL FO 135 μL buffer	PC 20 μL FO 130 μL buffer					
B		10 μL FQ 140 μL buffer									
C		10 μL FQ 140 μL buffer									

Table 16: Initial well plate setup including all required volumes for the Reporter Characterisation. Blue represents buffer volumes. Purple is for the volume of FQ complex needed. Orange is the volume of FO complex required.

	1	2	3	4	5	6	7	8	9	10	11
A	NC 50 μL buffer	0 μL O 50 μL buffer	2 μL O 48 μL buffer	4 μL O 46 μL buffer	6 μL O 44 μL buffer	8 μL O 42 μL buffer	10 μL O 40 μL buffer	PC 50 μL buffer	PC 50 μL buffer	PC 50 μL buffer	PC 50 μL buffer
B		0 μL O 50 μL buffer	2 μL O 48 μL buffer	4 μL O 46 μL buffer	6 μL O 44 μL buffer	8 μL O 42 μL buffer	10 μL O 40 μL buffer				
C		0 μL O 50 μL buffer	2 μL O 48 μL buffer	4 μL O 46 μL buffer	6 μL O 44 μL buffer	8 μL O 42 μL buffer	10 μL O 40 μL buffer				

Table 17: Outline of the required injection volumes of strand O and buffer for the initiation of the Reporter Characterisation reaction. Red represents the volume of strand O required and blue is for the buffer.

2. Verify concentrations of the strands using the Nanodrop
3. Use the thermal cycler to anneal the complexes
4. Dilute solutions down further to 200 nM solutions ready to be pipetted into the well plate

Note: For this reaction there will be no injection of reactants, hence the *Injection & Nuking* steps in the POLARstar Setup section (P8.3) can be ignored.

Reaction Step	Involved Strands/Complexes
Annealing	FQ, G _{init} O and FO complexes
Injecting	None
Nuking	None

Table 18: Outline of reaction steps and required strands for Leak Reaction testing.

Only the FQ and G_{init}O complexes are required for this reaction. The buffer used in this instance is the

combination TAE and NaCL buffer. **Table 18** outlines what DNA samples are used in each step of the leak reaction.

Table 19 outlines the volumes of each reactant in the well plate to perform this reaction. **Table 20** represents the desired concentrations of each sample in the well plate. Finish and save results from the reaction as outlined above.

	1	2	3	4	5	6	7	8	9	10
A	NC 200 μ L buffer	X₁ 10 μ L FQ 190 μ L buffer	X₂ 5 μ L G _{init} O 10 μ L FQ 185 μ L buffer	X₃ 10 μ L G _{init} O 10 μ L FQ 180 μ L buffer	X₄ 15 μ L G _{init} O 10 μ L pLFQ 175 μ L buffer	X₅ 20 μ L G _{init} O 10 μ L FQ 170 μ L buffer	PC 5 μ L FO 195 μ L buffer	PC 10 μ L FO 190 μ L buffer	PC 15 μ L FO 185 μ L buffer	PC 20 μ L FO 180 μ L buffer
B		X₁ 10 μ L FQ 190 μ L buffer	X₂ 5 μ L G _{init} O 10 μ L FQ 185 μ L buffer	X₃ 10 μ L G _{init} O 10 μ L FQ 180 μ L buffer	X₄ 15 μ L G _{init} O 10 μ L FQ 175 μ L buffer	X₅ 20 μ L G _{init} O 10 μ L FQ 170 μ L buffer				
C		X₁ 10 μ L FQ 190 μ L buffer	X₂ 5 μ L G _{init} O 10 μ L FQ 185 μ L buffer	X₃ 10 μ L G _{init} O 10 μ L FQ 180 μ L buffer	X₄ 15 μ L G _{init} O 10 μ L FQ 175 μ L buffer	X₅ 20 μ L G _{init} O 10 μ L FQ 170 μ L buffer				

Table 19: Overview of required volumes for setup of the well plate for the Leak Reaction testing. Purple represents the volume of FQ needed, green is for G_{init}O, orange outlines the volume of FO needed and blue is for the buffer.

	1	2	3	4	5	6	7	8	9	10
A	NC	X₁ 0 nM G _{init} O 10 nM FQ	X₂ 5 nM G _{init} O 10 nM FQ	X₃ 10 nM G _{init} O 10 nM FQ	X₄ 15 nM G _{init} O 10 nM FQ	X₅ 20 nM G _{init} O 10 nM FQ	PC 5 nM FO	PC 10 nM FO	PC 15 nM FO	PC 20 nM FO

Table 20: Well Plate setup with desired concentrations of each solution for Leak Reaction. Green represents the desired concentrations of the G_{init}O complex, purple indicates the concentrations of FQ complex and orange represents the concentrations of the FO complex.

P10. Additional Procedures

P10.1. Buffer Preparation

Task: Prepare two 50 mL buffer solutions; one salted - a combination of 1 x TAE and 1 M NaCl; and one unsalted, just TAE (used for diluting the stock solutions of the strands). Buffers are created using 50 M NaCl and 10 x TAE buffer stock solutions.

Create the following buffer solutions using the dilution equation (Equation P8.1, represented again here).

$$M_1V_1 = M_2V_2$$

1. Unsalted buffer: To create 1 x TAE (Tris-Acetate EDTA) buffer solution, dilute existing 10x stock solution with purified water. To do this, mix 5 mL of 10 x TAE with 45 mL of purified water in a falcon tube. Alternatively, use TAE prepared by laboratory tech.
2. Salted buffer: To create a combined 1 x TAE and 1 M NaCl buffer solution from stock solution, mix 5 mL 10 x TAE and 1 mL 10 M NaCL with 44 mL purified water in a falcon tube.

Data Analysis Procedure

In this document, we detail the procedure for converting the fluorescence values in arbitrary fluorescence units (AFU) to the concentration of the invader strand (X) in nM during the full strand displacement reaction. This involves a toehold exchange reaction that triggers a reporter duplex as defined in [P6](#).

F1. Remove Background Fluorescence

The first step involves removing the background fluorescence at each time point by subtracting the fluorescence value of the wells purely containing 1M NaCl in 1xTAE buffer from all recorded fluorescence values.

F2. Positive Control Reference

The second step aims to establish a reference value from the positive controls at each time point. Positive controls were recorded at 5nM, 10nM, 15nM and 20nM concentrations of FO. As we expect a maximum of 10nM FO to be formed during our reaction, we choose to define our sample values with respect to a positive control at 10nM. Therefore, we must calculate a robust estimate for the fluorescence value corresponding to 10nM FO at each time point. We expect the recorded fluorescence value of the positive controls to decline over time. Similarly, we assume that the ratio of the fluorescence at a certain time point ($p_X(t)$) to the reference fluorescence value established during initialisation ($p_{ref,X}$) is not affected by the concentration of the positive control. In other words, $\frac{p_5(t)}{p_{ref,5}} = \frac{p_{10}(t)}{p_{ref,10}} = \frac{p_{15}(t)}{p_{ref,15}} = \frac{p_{20}(t)}{p_{ref,20}}$.

During initialisation, once the fluorescence measurements had stabilised, we calculated the reference positive control values by averaging the fluorescence values recorded over approximately 10-15 minutes. After plotting these data points against concentration, we use least squares regression to fit a linear trendline to the data. We record the slope (M_{PC}) and offset (C_{PC}) of this trendline.

We average the value of $\frac{p_X(t)}{p_{ref,X}}$ for each concentration to find a reliable estimate for $\frac{p_{10}(t)}{p_{ref,10}}$. However, we can now use the fitted trend line to find the reference positive control fluorescence for each concentration. We then multiply by the fluorescence value corresponding to 10 nM to estimate the value of a 10 nM positive control at each time point as seen in [Equation F2.1](#).

$$\tilde{p}_{10}(t) = (M_{PC} \cdot 10nM + C_{PC}) \cdot \frac{1}{4} \sum_{X=5,10,15,20} \frac{p_X(t)}{M_{PC} \cdot XnM + C_{PC}} \quad (\text{F2.1})$$

F3. Converting Sample Fluorescence Values

Subsequently, in order to determine the concentration of FO in the sample wells we first find the ratio between the corresponding positive control, $\tilde{p}_{10}(t)$, and the sample fluorescence value, $\tilde{f}(t)$. We then multiply the fraction by 10 nM to approximate the concentration which we define as $g(t)$.

As determined in the FQ characterisation (see [D.2](#)), we expect the quenched reporter to contribute to the fluorescence. However, so far we have described the sample values in relation to the positive control values where the only duplex contributing to fluorescence is FO. Therefore, as seen in [Equation F3.1](#), we can use the fact that the sum of $[FQ]$ and $[FO]$ must be constant to derive an equation that accounts for the quenched reporter fluorescence. We assume a linear relationship between concentration and fluorescence as shown in [Figure 16](#) and so can use the gradients calculated during calibration, M_{FQ} and M_{FO} , to relate concentration

in nM to fluorescence in Arbitrary Fluorescence Units (AFU).

Conservation of mass:

$$[F_T] = [FQ](t) + [FO](t)$$

Sum of Fluorescence contribution:

$$\begin{aligned} M_{FO} \cdot g(t) &= M_{FQ}[FQ](t) + M_{FO}[FO](t) \\ &= M_{FQ}([F_T] - [FO](t)) + M_{FO}[FO](t) \\ &= M_{FQ}[F_T] + [FO](t) \cdot (M_{FO} - M_{FQ}) \end{aligned}$$

Isolate $[FO]$:

$$\begin{aligned} [FO](t) &= \frac{M_{FO} \cdot g(t) - M_{FQ} \cdot [F_T]}{M_{FO} - M_{FQ}} \\ &= \frac{g(t) - \frac{M_{FQ}}{M_{FO}}[F_T]}{1 - \frac{M_{FQ}}{M_{FO}}} \end{aligned} \tag{F3.1}$$

In order to determine a value of $[F_T]$, we assume the final recorded fluorescence after injecting a high concentration of the invader will correspond to all FQ being transformed to FO. Therefore, we estimate this value to be the sum of $[FQ]$ and $[FO]$ at any time point.

The final consideration we mitigated against was the contribution of excess incumbent strands in solution. When annealing the GO duplex, we introduced a 20% excess of O strands. We assume these strands trigger the quenched reporter at a much higher rate than the invader strand and so contribute to the fluorescence. Therefore, assuming the incumbent strands trigger the quenched reporter effectively instantaneously compared to the invader strands, we can use the negative control containing purely FQ and GO to estimate the concentration of excess O in the sample wells. We calculate $g_O(t)$ in the same way as $g(t)$ and assume that the concentration of O in the negative control is the same as in the sample wells. Therefore, accounting for the fluorescence contribution of FQ and using the $[F_T]$ value for the corresponding well, we can define the concentration of O in each sample well as in [Equation F3.2](#).

$$[FO]_O(t) = \frac{g_O(t) - \frac{M_{FQ}}{M_{FO}}[F_T]}{1 - \frac{M_{FQ}}{M_{FO}}} \tag{F3.2}$$

Therefore, we subtract the concentration of FO that has been produced due to the excess incumbent strand as seen in [Equation F3.3](#).

$$\begin{aligned} [FO]_X(t) &= [FO](t) - [FO]_O(t) \\ &= \frac{g(t) - \frac{M_{FQ}}{M_{FO}}[F_T] - g_O(t) + \frac{M_{FQ}}{M_{FO}}[F_T]}{1 - \frac{M_{FQ}}{M_{FO}}} \\ &= \frac{g(t) - g_O(t)}{1 - \frac{M_{FQ}}{M_{FO}}} \end{aligned} \tag{F3.3}$$

F4. Approximating Rate Constant and Invader Concentration

We utilize the lsqcurvefit MATLAB function which uses nonlinear least-squares optimization to fit the two parameters defined in the ODE shown in [Equation F4.1](#). $[X_T]$ corresponds to the total concentration of $[G_iX]$ i.e. the concentration of invader that eventually displaces the incumbent strand and k corresponds to the rate constant. All code can be found in the Data Analysis folder of our GitHub Repository linked [here](#).

$$\begin{aligned}\frac{d[FO]}{dt} &= k[FQ][O] \\ &= k([F_T] - [FO])([O_T] - [FO]) \\ &= k([F_T] - [FO])([X_T] - [FO]) \\ \frac{d[G_iX]}{dt} &= k([F_T] - [G_iX])([X_T] - [G_iX])\end{aligned}\tag{F4.1}$$

Constants:

$$\begin{aligned}[F_T] &= [FQ](t) + [FO](t) \\ [O_T] &= [FO](t) + [O](t) = [G_iX](t) + [X](t) = [X_T]\end{aligned}$$

Parameters:

$$\begin{aligned}k &: \text{Rate Constant} \\ [X_T] &: \text{Initial Injected Invader Concentration}\end{aligned}$$